Antagonism between splicing and microprocessor complex dictates the serum-induced processing of lnc-*MIRHG* for efficient cell cycle reentry

QINYU SUN,[1] QINYU HAO,[1] YO-CHUEN LIN,[1] YOU JIN SONG,[1] SUSHANT BANGRU,[2,3] WAQAR ARIF,[2] VIDISHA TRIPATHI,[1,10] YANG ZHANG,[4] JUNG-HYUN CHO,[5] SUSAN M. FREIER,[6] LISA M. JENKINS,[7] JIAN MA,[4] JE-HYUN YOON,[5] AUINASH KALSOTRA,[2,3,8] ASHISH LAL,[9] SUPRIYA G. PRASANTH,[1] and KANNANGANATTU V. PRASANTH[1,3]

[1]Department of Cell and Developmental Biology, University of Illinois at Urbana-Champaign, Urbana, Illinois 61801, USA
[2]Department of Biochemistry, University of Illinois at Urbana-Champaign, Urbana, Illinois 61801, USA
[3]Cancer Center at Illinois, University of Illinois at Urbana-Champaign, Urbana, Illinois 61801, USA
[4]School of Computer Science, Carnegie Mellon University, Pittsburgh, Pennsylvania 15213, USA
[5]Department of Biochemistry and Molecular Biology, Medical University of South Carolina, Charleston, South Carolina 29425, USA
[6]Ionis Pharmaceuticals Inc., Carlsbad, California 92008, USA
[7]Laboratory of Cell Biology, Center for Cancer Research, National Cancer Institute, NIH, Bethesda, Maryland 20892, USA
[8]Carl R. Woese Institute for Genomic Biology, University of Illinois at Urbana-Champaign, Urbana, Illinois 61801, USA
[9]Regulatory RNAs and Cancer Section, Genetics Branch, Center for Cancer Research, National Cancer Institute, Bethesda, Maryland 20892, USA

ABSTRACT

Cellular quiescence and cell cycle reentry regulate vital biological processes such as cellular development and tissue homeostasis and are controlled by precise regulation of gene expression. The roles of long noncoding RNAs (lncRNAs) during these processes remain to be elucidated. By performing genome-wide transcriptome analyses, we identify differential expression of several hundreds of lncRNAs, including a significant number of the less-characterized class of microRNA-host-gene (*MIRHG*) lncRNAs or lnc-*MIRHGs*, during cellular quiescence and cell cycle reentry in human diploid fibroblasts. We observe that *MIR222HG* lncRNA displays serum-stimulated RNA processing due to enhanced splicing of the host nascent pri-*MIR222HG* transcript. The pre-mRNA splicing factor SRSF1 negatively regulates the microprocessor-catalyzed cleavage of pri-miR-222, thereby increasing the cellular pool of the mature *MIR222HG*. Association of SRSF1 to pri-*MIR222HG*, including to a mini-exon, which partially overlaps with the primary miR-222 precursor, promotes serum-stimulated splicing over microRNA processing of *MIR222HG*. Further, we observe that the increased levels of spliced *MIR222HG* in serum-stimulated cells promote the cell cycle reentry post quiescence in a microRNA-independent manner. *MIR222HG* interacts with *DNM3OS*, another lncRNA whose expression is elevated upon serum-stimulation, and promotes cell cycle reentry. The double-stranded RNA binding protein ILF3/2 complex facilitates *MIR222HG:DNM3OS* RNP complex assembly, thereby promoting *DNM3OS* RNA stability. Our study identifies a novel mechanism whereby competition between the splicing and microprocessor machinery modulates the serum-induced RNA processing of *MIR222HG*, which dictates cell cycle reentry.

Keywords: quiescence; cell cycle; lncRNAs; microRNA-host genes

INTRODUCTION

Cell proliferation is a complex biological process that is controlled by differential gene and protein expression. A typical eukaryotic cell cycle consists of four consecutive stages: G1, S (synthesis), G2, and M (mitotic) phases (Harashima et al. 2013). Additionally, there exist three types of nondividing cell states: terminally differentiated, senescent, and quiescent. Among them, quiescence/G0 is unique due to its reversibility. Cells in quiescence

[10]**Present address:** National Center for Cell Science, Pune 411007, India
Corresponding author: kumarp@illinois.edu
Article is online at http://www.rnajournal.org/cgi/doi/10.1261/rna.075309.120.

temporarily exit the cell cycle and can resume cell division capacity by entering back to G1 upon environmental cues (Coller 2007; So and Cheung 2018). In higher multicellular organisms, undergoing cellular quiescence is essential for the regulation of tissue regeneration and homeostasis, immune responses, and aging (Yusuf and Fruman 2003; Liu et al. 2007; Lemons et al. 2010; Coller 2011; Bainbridge 2013; Yao 2014). In the context of disease, cancer stem cells remain in quiescent state and resume proliferation during tumor reoccurrence (Cheung and Rando 2013). Dysregulation of cellular quiescence is correlated with proliferation-related diseases such as fibrosis, immune disorders, and cancer (Liu et al. 2007; Lemons et al. 2010; Coller 2011; Yao 2014). A deep understanding of quiescence induction and maintenance, and further exit out of quiescence or cell cycle reentry, will allow the discovery of therapeutic targets for treating quiescence-related diseases.

Earlier studies have established the roles of signaling pathways/protein factors/microRNAs (miRNAs) in quiescence maintenance and cell cycle reentry. For instance, certain metabolic processes are found to be reprogrammed in quiescent cells (Lemons et al. 2010; Laporte et al. 2011; Valcourt et al. 2012). Likewise, various signaling pathways are highly regulated during quiescence (Coller et al. 2006; Lemons et al. 2010; Valcourt et al. 2012; So and Cheung 2018). Several groups have also reported aberrant levels and/or functions of protein-coding genes and miRNAs during quiescence establishment or cell cycle reentry (Gos et al. 2005; Coller et al. 2006; Coller 2007, 2011; Liu et al. 2007; Cheung et al. 2012; Suh et al. 2012; Cheung and Rando 2013; Polioudakis et al. 2013; Yao 2014; Martinez et al. 2017). Long noncoding RNAs (lncRNAs) have been shown, by us and others, to play important roles in cell cycle progression and therefore have the potential to regulate quiescence and cell cycle reentry. However, only few studies so far have reported the role of lncRNAs in these processes (Venkatraman et al. 2013; Bierhoff et al. 2014).

LncRNAs are noncoding RNAs that are longer than 200 nt, most of which do not code for any proteins or peptides. They are ubiquitously found in many species from prokaryotes to eukaryotes and can play diverse roles in multiple biological events including differentiation, cell cycle progression, immune response, apoptosis, and diseases (Kitagawa et al. 2013; Flynn and Chang 2014; Fang and Fullwood 2016; Li et al. 2016; Schmitt and Chang 2016; Chen et al. 2017). LncRNAs function in both the nucleus and the cytoplasm via various mechanisms such as regulating nuclear structure, chromatin, gene transcription, RNA stability, or translation, often by interacting with other protein/RNA/DNA elements (Wang and Chang 2011; Marchese et al. 2017; Noh et al. 2018; Sun et al. 2018a). Several lncRNAs can also produce short and functional peptides (Choi et al. 2019).

Some lncRNA genes display intriguing genomic structures wherein they harbor miRNA genes in their gene loci and are therefore categorized as "*microRNA-host-gene* lncRNAs (lnc-*MIRHG*s)." MiRNAs are ~22 nt noncoding RNAs that play crucial roles in posttranscriptional regulation of gene expression (Ameres and Zamore 2013). Most miRNAs are encoded within protein-coding or long noncoding genes (Berezikov et al. 2007a; Kahl 2009; Monteys et al. 2010). A significant fraction of miRNAs (17.5%) in humans are encoded within lnc-*MIRHG*s (Dhir et al. 2015b). Earlier studies have reported that lnc-*MIRHG*s can serve as diagnosis/prognosis markers and also play regulatory roles in various cellular processes (Augoff et al. 2012; Morenos et al. 2014; Montes et al. 2015; Kato et al. 2016; Molinari et al. 2016; Su et al. 2018). These studies have brought crucial insights into the significance of lnc-*MIRHG*s. However, most of these studies have focused on their role merely as a source of miRNA synthesis. On the other hand, several recent studies, including work from our laboratory, have provided compelling evidence demonstrating miRNA-independent roles of the mature and processed lnc-*MIRHG*s (Ng et al. 2013; Tseng et al. 2014; Colombo et al. 2015; Raveh et al. 2015; Shih et al. 2017; Sun et al. 2018b; Du et al. 2019; Profumo et al. 2019). For instance, we have demonstrated that lncRNA *MIR100HG*, whose gene locus hosts miR-125-b1 and miR-100, regulates cell cycle progression by modulating the activity of RNA-binding protein HuR in a miRNA-independent manner (Sun et al. 2018b). Two other recent studies described *MIR205HG*'s role in regulating basal-luminal differentiation as well as the production of growth hormone and prolactin (Du et al. 2019; Profumo et al. 2019).

At present, very little is known about the function of lnc-*MIRHG*s during quiescence and cell cycle reentry. The major "road-block" to such studies is the lack of genome-wide analysis of lncRNA expression, including lnc-*MIRHG,* during these processes. Keeping this in mind, we performed a systematic transcriptome profiling to identify differentially expressed protein-coding and lncRNA genes during cellular quiescence and subsequent reentry into the cell cycle in normal human diploid fibroblasts. From this, we identified several dynamically regulated lnc-*MIRHG*s, and further focused on mechanistic studies of *MIR222HG,* which showed enhanced expression during cell cycle reentry. We found that the spliced (and mature) *MIR222HG* levels were significantly elevated in serum-stimulated cells due to the enhanced processing of pri-*MIR222HG* transcripts, mediated by the pre-mRNA splicing factor SRSF1. We further demonstrated that the spliced *MIR222HG* facilitated cell cycle reentry in a miRNA-independent manner. Mechanistic studies revealed that *MIR222HG* forms an RNP (Ribonucleoprotein) complex along with another lncRNA *DNM3OS* and ILF3/ILF2 complex to stabilize *DNM3OS*, which in turn is instrumental in modulating serum-stimulated cell cycle reentry.

RESULTS

Transcriptome profiling of quiescent and serum-stimulated cells reveals differential expression of both protein- and noncoding genes

Cellular quiescence can be induced experimentally via serum deprivation, loss of adhesion, or cell contact inhibition (Coller et al. 2006). In the present study, we triggered cellular quiescence in normal human diploid lung fetal fibroblast WI-38 cells by serum starvation (Fig. 1A). WI-38 cells become quiescent after 72-h of serum starvation, reflected by the almost undetectable populations of S-phase or G2/M phase cells (Fig. 1B). Quiescent WI-38 cells reenter the cell cycle upon serum stimulation that results in increase in S and G2/M phase populations (Fig. 1B).

To understand the roles of lncRNAs in cellular quiescence and cell cycle reentry, we performed RNA-seq from asynchronous, quiescent, and serum-stimulated (3 and 6 h of serum-stimulation post quiescence) WI-38 cells. We reasoned that genes that play vital roles in cell cycle reentry would show differential expression during the early time points of serum stimulation. Hence, we chose 3 and 6 h of serum stimulation as time points for RNA isolation. The polyA$^+$ paired-end RNA-seq was performed in biological duplicates with high-quality, high-depth, and high reproducibility between replicates (Supplemental Fig. S1A,B). We detected the expression of 17,640 genes including 13,574 protein-coding and 4066 noncoding genes, in which 3889 genes were annotated as lncRNAs (Supplemental Fig. S1C; Supplemental Table S1). We observed dramatic changes in both complete transcriptome

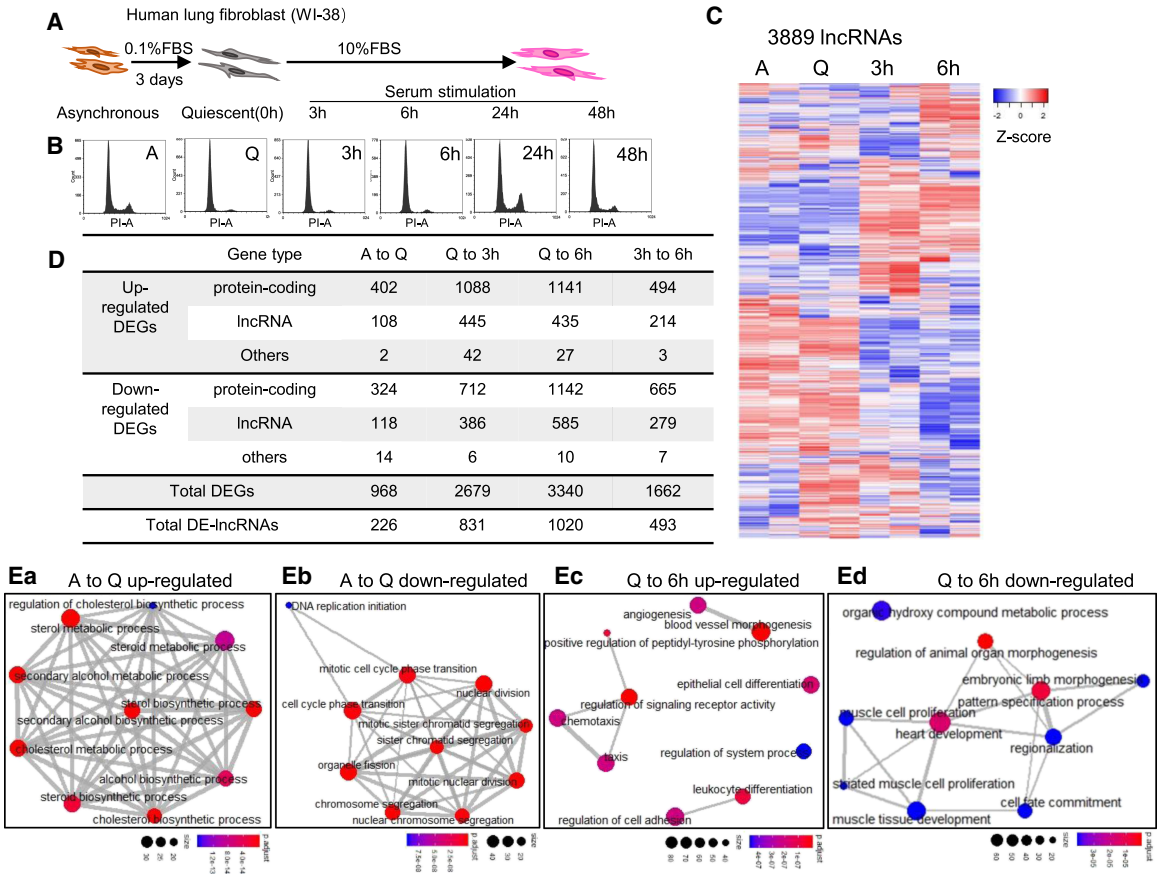

	Gene type	A to Q	Q to 3h	Q to 6h	3h to 6h
Up-regulated DEGs	protein-coding	402	1088	1141	494
	lncRNA	108	445	435	214
	Others	2	42	27	3
Down-regulated DEGs	protein-coding	324	712	1142	665
	lncRNA	118	386	585	279
	others	14	6	10	7
Total DEGs		968	2679	3340	1662
Total DE-lncRNAs		226	831	1020	493

FIGURE 1. Transcriptome landscape of human lung fibroblasts during quiescence and cell cycle reentry. (*A*) Schematic of inducing WI-38 cellular quiescence and cell cycle reentry using serum starvation and serum stimulation method. (*B*) PI-flow cytometry analyses in WI-38 during cellular quiescence and cell cycle reentry. A: asynchronous; Q: quiescent; 3 h/6 h/24 h/48 h: corresponding serum stimulation time postserum-starvation. (*C*) Heatmaps showing the relative expression levels of 3889 lncRNAs detected from RNA-seq. Biological duplicates from four time points are represented. Genes (rows of heatmap) are hierarchically clustered using average-linkage clustering method. (*D*) Table representing the number of differentially expressed genes (DEGs) detected from multiple comparisons between RNA-seq samples. Detailed DEG information is available in Supplemental Table S2. (*E*) Gene ontology (GO) analyses showing the top enriched biological processes of (*a*) up-regulated DEGs and (*b*) down-regulated DEGs from asynchronous to quiescence, as well as (*c*) up-regulated DEGs and (*d*) down-regulated DEGs from quiescence to 6 h serum stimulation. Nodes represent the gene size in each biological process, edges represent the overlapping of genes in different processes. Full GO analyses results are listed in Supplemental Table S3.

profile (17,640 genes) and lncRNA transcriptome profile (3889 genes) of quiescent and serum-stimulated fibroblasts (Fig. 1C; Supplemental Fig. S1D).

We then performed statistical analyses to identify differentially expressed genes (DEGs; $|\log_2$ (fold change)$| > 1$ and FDR < 0.05) by comparing different RNA-seq samples, including asynchronous (A) to quiescence (Q) (A to Q), quiescence to serum stimulation (SS) (Q to 3 h SS, Q to 6 h SS), and 3 h SS to 6 h SS. We identified the differential expression of ~1000 to ~3000 genes during these cell cycle transitions (968 DEGs from A to Q, 2679 from Q to 3 h SS, 3340 from Q to 6 h SS, 1662 from 3 h to 6 h SS), in which ~20%–30% of them were lncRNAs (226 between A to Q, 831 between Q to 3 h SS, 1020 between Q to 6 h SS, 493 between 3 h to 6 h SS) (Fig. 1D; Supplemental Table S2). The differential expression of a significant number of lncRNAs during quiescence or cell cycle reentry implies that lncRNAs play vital roles during such cell cycle transitions.

To understand the biological processes that are involved in cellular quiescence and subsequent cell cycle reentry, we performed gene set enrichment analysis (GSEA) and gene ontology (GO) analyses. GSEA showed that multiple quiescence-associated processes were regulated between asynchronous (A) to quiescent (Q) states, exemplified by reduced rRNA processing (Supplemental Fig. S1Ea; Supplemental Table S3). We then performed GO analysis by stratifying DEGs into up-regulated and down-regulated groups. During A to Q transition, several key metabolic processes were found to be activated (Fig. 1Ea; Supplemental Table S3). On the contrary, genes controlling cell cycle-/cell division-related events showed consistent down-regulation in quiescent cells (Fig. 1Eb; Supplemental Table S3). Pathway analyses also revealed key pathways that were affected during quiescence establishment, including the cell cycle (Supplemental Fig. S1Fa; Supplemental Table S3). Similarly, serum-stimulated cells exhibited enhanced levels of processes such as rRNA processing, MAPK cascade, and extracellular matrix organization (Supplemental Fig. S1Eb–d; Supplemental Table S3). In addition, up-regulated DEGs in serum-stimulated cells (Q to 6 h SS) participate in biological processes such as chemotaxis and angiogenesis, whereas genes controlling morphogenesis and development seem to be down-regulated during serum stimulation (Fig. 1Ec,d; Supplemental Table S3). We also observed that pathways controlling cell growth, metabolism, and development (MAPK/Ras/Hippo/PI3K-Akt pathways) showed significant changes during early serum response (Supplemental Fig. S1Fb,c; Supplemental Table S3).

The genome-wide transcriptome landscape analyses revealed that cells undergo complex, precise, and rapid changes in gene expression during both quiescence induction and exit out of quiescence. However, the role of lncRNAs during such processes is least understood. The large number of differentially expressed lncRNAs identified in this study hence serves as a useful resource for further mechanistic studies.

Genome-wide analysis of miRNA host genes identifies potential lnc-*MIRHG*s as regulators for cell cycle reentry

Earlier studies have uncovered the role of miRNAs in promoting/repressing quiescence (Cheung et al. 2012; Suh et al. 2012; Cheung and Rando 2013; Polioudakis et al. 2013). However, very little is known about the function of lncRNAs that are processed from miRNA-host gene loci (termed as lnc-*MIRHG*s), during quiescence and serum stimulation. To identify the lnc-*MIRHG* repertoire in the human genome, we performed a genome-wide screen to categorize the miRNAs and *MIRHG*s in the recent version of the human genome assembly GRCh38 (p12.v94). We classified miRNAs based on their relative location to the host genes (Fig. 2A). Our genomic analyses revealed that ~2/3 of human miRNAs (1263 out of 1879) were "intragenic miRs" and are encoded within 1149 host genes (*MIRHG*s), out of which 224 are composed of lncRNAs (lnc-*MIRHG*s). Furthermore, we found that most of the intragenic miRNAs (72%, 907 out of 1263) reside within the introns of *MIRHG*s ("intronic-miRs"), and 17% were located in the exonic regions ("exonic-miRs"). Interestingly, ~5% (57 out of 1263) of miRNAs were located at exon–intron junctions of protein-coding or lncRNA genes (Fig. 2B, C; Supplemental Tables S4, S5). Such miRNAs were previously identified as "SO-miRs" (splice site overlapping miRNAs), so we kept the same nomenclature (Mattioli et al. 2013, 2014; Pianigiani et al. 2018). Finally, the majority of *MIRHGs* (1028 out of 1149) host one miRNA and a small fraction of them contains multiple miRNAs (Supplemental Fig. S2A; Supplemental Table S5).

Eight hundred and seventy-five *MIRHG*s were expressed in WI-38 cells, wherein 91 belonged to the lnc-*MIRHG* repertoire (Fig. 2D; Supplemental Fig. S2B). We examined the differential expression (DE) of *MIRHG*s during quiescence and serum stimulation and further focused on the differentially expressed lnc-*MIRHG*s (DE-lnc-*MIRHG*s) (Fig. 2E; Supplemental Table S5). By this, we identified six DE-lnc-*MIRHG*s from asynchronous to quiescent transition, 18 DE-lnc-*MIRHG*s from quiescence to 3 h serum stimulation, 20 DE-lnc-*MIRHG*s from quiescence to 6 h serum stimulation (SS), and 8 DE-lnc-*MIRHG*s from 3 h SS to 6 h SS (Fig. 2E,F; Supplemental Fig. S2C).

LncRNA *MIR222HG* is induced during cell cycle reentry post cellular quiescence

Based on the existing knowledge in the case of protein-coding genes, we hypothesized that early serum-induced lncRNA genes play crucial roles in regulating cell cycle reentry. Among the several up-regulated DE-lnc-*MIRHG*s

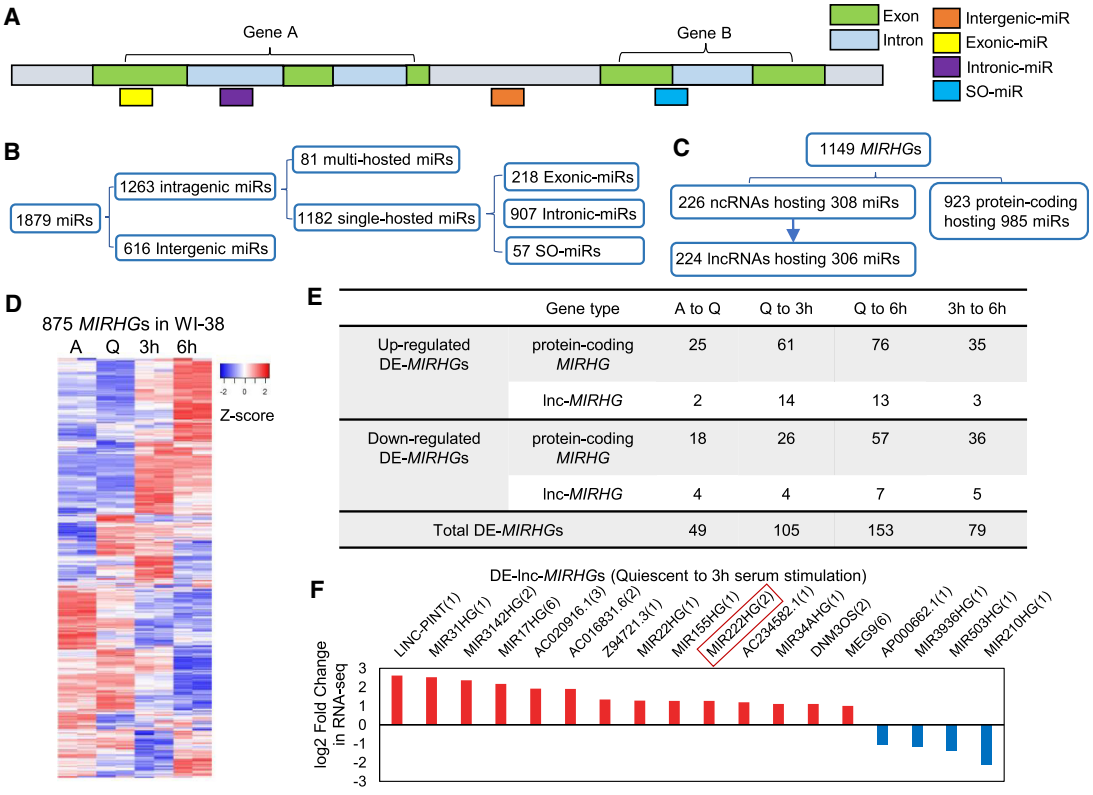

	Gene type	A to Q	Q to 3h	Q to 6h	3h to 6h
Up-regulated DE-*MIRHG*s	protein-coding *MIRHG*	25	61	76	35
	lnc-*MIRHG*	2	14	13	3
Down-regulated DE-*MIRHG*s	protein-coding *MIRHG*	18	26	57	36
	lnc-*MIRHG*	4	4	7	5
Total DE-*MIRHG*s		49	105	153	79

FIGURE 2. *MIRHG*s show dynamic expression during cellular quiescence and upon cell cycle reentry. (*A*) Schematic showing different types of miRNAs (miRs) categorized in this study. Detailed list is available in Supplemental Table S4. (*B*) Categorization of miRNAs (miRs) in human genome GRCh38 version in terms of their relative locations to host genes (*MIRHG*s). Detailed list is shown in Supplemental Table S4. (*C*) Categorization of all identified miRNA host genes (*MIRHG*s) in human genome GRCh38 version. Detailed list is shown in Supplemental Table S5. (*D*) Heatmap showing the relative expression levels of 875 *MIRHG*s that are expressed in WI-38 RNA-seq. Duplicates are represented. Genes (rows of heatmap) are hierarchically clustered using average-linkage clustering method. (*E*) Table representing the number of differentially expressed *MIRHG*s (DE-*MIRHG*s) detected from multiple comparisons between RNA-seq samples. Detailed DE-*MIRHG* information is available in Supplemental Table S5. (*F*) Fold change ($\log_2$ scale) of 18 DE-lnc-*MIRHG*s from quiescent to 3-h serum stimulation. Numbers in the parentheses refer to the number of miRNAs encoded within each lnc-*MIRHG*. See Supplemental Table S5 for detailed DE-lnc-*MIRHG*s information.

from quiescence to 3 h serum stimulation, we focused our investigations on *MIR222HG* for several reasons. *MIR222HG* (ENSG00000270069 from Ensembl, lnc-CXorf36-46:7 from LNCipedia) is transcribed from the X-chromosome and it is up-regulated upon 3 h and 6 h of serum stimulation (Fig. 2F; Supplemental Fig. S2Cb; Supplemental Table S5). The *MIR222HG* gene locus encodes two miRNAs, miR-221 and miR-222 (Fig. 3A), both of which were previously reported to play roles in cell proliferation and cancer progression (Felli et al. 2005; Medina et al. 2008; Cardinali et al. 2009; Chun-Zhi et al. 2010; Garofalo et al. 2012; Li et al. 2014). In addition, lncRNA *MIR222HG* was also reported to play a pro-tumorigenic role (Sun et al. 2018c), further implying that its induction during serum stimulation could promote cell proliferation. The existing Ensembl gene annotation indicates that *MIR222HG* contains two exons and a long intron, within which both miR-221 and 222 reside (Fig. 3A, ENSG 00000270069, GENCODE track). RNA-seq revealed significant number of reads from the 3′ end of the last intron, spanning miR-221 and miR-222 (Supplemental Fig. S3A), implying intron retention. Our high-depth RNA-seq (~100 million paired reads/sample) analyses revealed that the spliced (and mature) *MIR222HG* expressed in WI-38 cells contained an unannotated 44 bp mini-exon, which partially overlapped with the 5′ end of the primary precursor of miR-222 (Fig. 3A; Supplemental Fig. S3Ba, b). The 10 bp at the 3′ end of the 44 bp exon is located just upstream of the lower stem of the pri-miR-222 hairpin structure and formed imperfect complementarity with the 3′ end of the pri-miR-222 sequence (Fig. 3B).

This observation indicates that in WI-38 cells, miR-222 is expressed as a SO-miRNA instead of an intronic miRNA. In support of this, an earlier study had categorized miR-222 as a SO-miRNA in the *Bos tauros* genome (Melamed et al. 2013). In addition, we have identified the transcription start site of *MIR222HG* isoform in WI-38 cells. The 5′ end of *MIR222HG* (based on RNA-seq reads and 5′ RACE), which is different from the current GENCODE/Ensembl annotation, is located ~24 kb upstream of

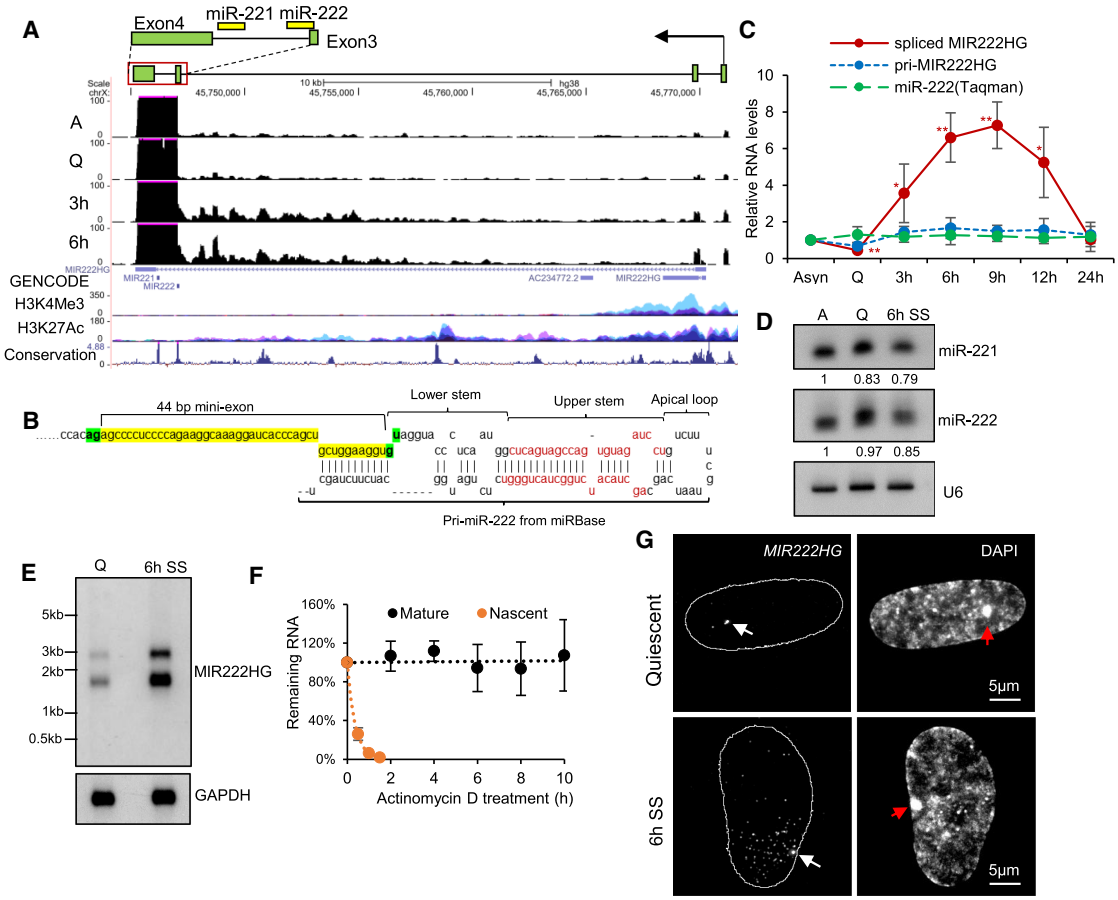

FIGURE 3. *MIR222HG* is induced during the cell cycle reentry post cellular quiescence. (*A*) UCSC genomic browser view of *MIR222HG* genomic locus and RNA-seq coverage tracks in WI-38 cells. *Y*-axis displays the reverse strand of BigWig (bw) files. Max value of *y*-axis is set at 100 for a better visualization of exons 1–3 of *MIR222HG*. Full display of the last exon's signal is shown in Supplemental Figure S3A. H3K4Me3 and H3K27Ac mark tracks contain all of the seven ENCODE cell lines. Conservation track presents Vertebrate Multiz Alignment & Conservation (100 Species). Schematic of the ~1.3 kb *MIR222HG* isoform expressed in WI-38 is drawn on the *top* to represent its genomic location; regions spanning the last two exons and last intron are presented in detail. The genomic positions of miRs are shown as yellow rectangles. (*B*) Schematic of the 44 bp mini-exon genomic position with respect to the hairpin structure of primary miR-222. Nucleotide sequence of the 44 bp mini-exon is highlighted in yellow. The 5′GU and 3′AG spliced site on either side of the mini-exon are highlighted in green. Sequences in red represent the miRNA duplex of miR-222. Primary miR-222 structure is obtained from miRbase database (http://www.mirbase.org/cgi-bin/mirna_entry.pl?acc=MI0000299). (*C*) Relative levels of *MIR222HG* (pri- and mature forms) and miR-222 (TaqMan assay) in WI-38s during quiescence and various time points (h/hours) postserum stimulation. (*D*) Northern blot to detect human miR-221 and miR-222 from asynchronous, quiescent, and 6-h postserum-stimulated WI-38 cells. U6 is used as loading control. Relative levels of miR-221 and miR-222 are included *below* the blots, by normalization to U6 levels and comparison to asynchronous sample. Quantification is performed using ImageJ. (*E*) Northern blot to detect *MIR222HG* using polyA$^+$ RNA from quiescent and 6-h serum-stimulated WI-38 cells. *GAPDH* is used as loading control. *MIR222HG* construct used for probe preparation contains sequence from exons 2–4; please see cloning primer position in Supplemental Figure S3D. (*F*) RNA stability analyses of mature and pri-*MIR222HG*. RNA is extracted from WI-38s treated by actinomycin D for different time points. The levels of *MIR222HG* RNA (pri-*MIR222HG* as well as mature *MIR222HG*) are quantified via RT-qPCR and compared to 0 h time point to calculate the remaining levels of RNA. (*G*) Single molecule RNA-FISH (smRNA-FISH) to detect *MIR222HG* in quiescent and serum stimulated WI-38 cells. DNA is counterstained with DAPI. Contour represents the nuclei location. The magnification bar represents 5 μm. White arrows indicate transcription site and red arrows indicate Barr body. (*) $P \le 0.05$, (**) $P \le 0.01$, (***) $P \le 0.001$, (****) $P \le 0.0001$ by two-tailed Student's *t*-test, $n = 3$ for all figures. Error bars represent standard deviation.

miR-222 and the promoter of *MIR222HG* is decorated with chromatin marks (H3K4Me3 and H3K27Ac) associated with active transcription (Fig. 3A). We confirmed the 5′ and 3′ ends of *MIR222HG* by RACE experiment, and the full-length of the annotated spliced/mature *MIR222HG* was ~1.3 kb (please see the full sequence in Supplemental File). The PhyloCSF score and ribosome footprint from ribo-seq signals indicated that *MIR222HG* did not code for any protein (Supplemental Fig. S3A). Further, ribosome fractionation followed by RT-qPCR analyses showed that *MIR222HG* was majorly associated with the monosome fraction, whereas the protein-coding *GAPDH* mRNA showed a strong association with heavy polysome fractions (Supplemental Fig. S3C). In summary,

MIR222HG is a multiexonic lnc-*MIRHG* containing a 44 bp mini-exon partially overlapping with the primary precursor of miR-222.

We next performed RT-qPCR to quantitate the relative levels of both nascent and mature *MIR222HG* using primers from exonic or inronic regions or exon–intron or exon–exon junctions of *MIR222HG* (Supplemental Fig. S3D). The pri-*MIR222HG* transcript, detected by the exon–intron junction primer, showed moderate up-regulation (approximately twofold) from quiescence to 3-h serum stimulation (Fig. 3C, blue line) and the levels remained stable afterward. Primers detecting either the intronic or exonic regions of *MIR222HG* also displayed similar patterns (Supplemental Fig. S3D,E). However, the spliced, mature *MIR222HG* was strongly up-regulated in serum-stimulated cells (eightfold from Q to 3 h SS, 15-fold from Q to 6 h SS), as detected by two distinct sets of exon–exon junction primers (Fig. 3C, red line, Supplemental Fig. S3D,E). This data implies that the addition of serum only moderately enhanced the transcription of *MIR222HG* but dramatically elicited the posttranscriptional processing of pri-*MIR222HG* to produce spliced *MIR222HG*. Since both miR-221 and miR-222, encoded in the *MIR222HG*, are known to play broad functions in multiple cellular processes including cell proliferation and quiescence (Felli et al. 2005; Medina et al. 2008; Cardinali et al. 2009; Chun-Zhi et al. 2010; Mayoral et al. 2011; Garofalo et al. 2012; Li et al. 2014), we examined if they show altered expression during serum stimulation. Both quantitative TaqMan assay and Northern blot analyses showed that miR-221 and miR-222 levels remained unchanged among asynchronous, quiescent, and serum-stimulated samples, suggesting that their levels were not coregulated with the mature *MIR222HG* (Fig. 3C green line, Fig. 3D). Northern blot using poly(A)$^+$ RNA detected two discrete bands at ~1.5 kb and <3 kb of *MIR222HG* in both quiescent and 6 h SS WI-38 cells (Fig. 3E). We reasoned that the 1.5 kb RNA coded for the mature poly-adenylated *MIR222HG*, whereas the <3 kb band most likely corresponded to the miRNA-bearing intron 3-retained isoform of *MIR222HG*. Both isoforms displayed enhanced expression in serum-stimulated cells (Fig. 3E). Northern blot data further supported the RT-qPCR analyses that showed increased levels of spliced/mature and not the pri-*MIR222HG* transcripts upon serum stimulation.

Earlier studies have reported Drosha-mediated transcription termination of noncoding *MIRHGs* in human cells (Dhir et al. 2015a; Pianigiani et al. 2018). In such a scenario, cleavage of pri-*MIRHG* by Drosha results in the generation of poly(A)$^-$ and unstable *MIRHG* transcripts of no apparent function. Unlike the other lnc-*MIRHG* transcripts that were identified in earlier studies, *MIR222HG* contains a discrete poly(A)$^+$ tail. We further determined the stability of *MIR222HG* by transcription inhibition followed by a chase experiment. We observed that spliced *MIR222HG* constituted a very stable pool compared to the nascent form of *MIR222HG*, pri-*MIR222HG* (Fig. 3F). Pri-*MIR222HG* is relatively abundant, present at 300–500 copies/cell and predominantly localized in the nucleus, whereas the low-abundant spliced *MIR222HG* was localized in both nuclear and cytoplasmic compartments (Supplemental Fig. S3F,G). We next performed single-molecule fluorescence RNA in situ hybridization (smRNA-FISH) to determine the cellular localization of *MIR222HG* in quiescent and serum-stimulated cells. smRNA-FISH revealed that *MIR222HG* was expressed only from the active X-chromosome, as observed by a single prominent locus, reminiscent of the transcription site (Fig. 3G; white arrow). No smRNA-FISH signal was observed on the DAPI-rich inactive-X-chromosome (Barr body) (Fig. 3G, red arrows). In the quiescent cell nucleus, most of *MIR222HG* RNA decorated at the transcription site, and this fraction of RNA could represent the nascent transcripts, pri-*MIR222HG*. In serum-stimulated cells, we continued to see enrichment of *MIR222HG* RNA at its transcription site. In addition, we observed 20–30 bright RNA spots in the nucleoplasm, located in proximity to the *MIR222HG* transcription site (Fig. 3G; Supplemental Fig. S3H). Since RNA splicing is predominantly a cotranscriptional event, we concluded that the RNA spots that were dispersed in the nucleoplasm represent spliced and mature *MIR222HG*. Thus, the smRNA-FISH results further confirmed our molecular analyses (RNA-seq and RT-qPCR) that serum stimulation enhanced the RNA splicing of *MIR222HG*. Both smRNA-FISH (Supplemental Fig. S3H) and RT-qPCR (Fig. 3C) results showed reduced expression of mature *MIR222HG* post 12 h serum stimulation (compared to 6 h). This result implies that serum stimulation enhances the splicing of pri-*MIR222HG* that are concentrated at its site of transcription, whereas the spliced, mature *MIR222HG* diffuse into the nucleoplasm.

SRSF1 antagonizes Drosha/DGCR8 for spliced *MIR222HG* biogenesis upon serum stimulation

Increased levels of spliced *MIR222HG* in serum-stimulated cells indicate serum-responsive posttranscriptional processing of pri-*MIR222HG*. An earlier study reported that pre-mRNA splicing factor SRSF1 (Serine/arginine-rich splicing factors) promotes the Drosha-mediated cleavage of miR-222 in HeLa cells (Wu et al. 2010). SRSFs constitute a conserved family of essential pre-mRNA splicing factors, which bind to the exonic regions on pre-mRNAs by recognizing exonic splicing enhancers (ESEs) (Busch and Hertel 2012). RBPmap prediction analyses identified a consensus SRSF1 binding site (ugrwgvh/ugcugga) within the 44 bp mini-exon (Paz et al. 2014). The publicly available eCLIP data set from human HepG2 cells (ENCODE project ENCSR989VIY) displayed significant binding of SRSF1 at the 44 bp mini-exon (Fig. 4A). We therefore hypothesized that the increased binding of SRSF1 on the mini-exon in serum-stimulated cells could facilitate the recruitment of the

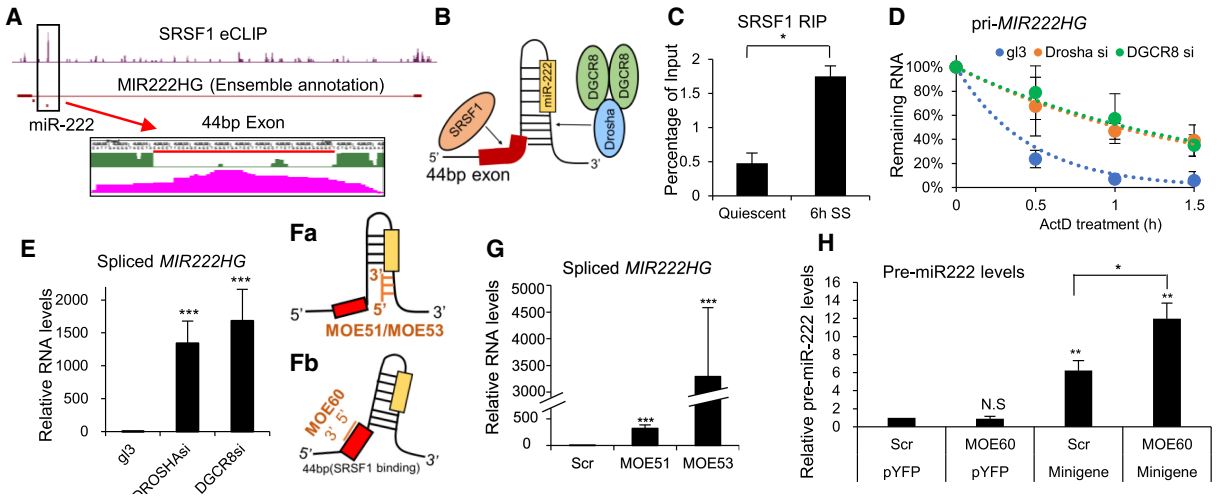

FIGURE 4. Mature spliced *MIR222HG* lncRNA is processed via the competition between SRSF1 and microprocessor complex. (*A*) SRSF1 eCLIP signal from HepG2 cells at the 44 bp mini-exon position. The peak at the 44 bp mini-exon is zoomed in and displayed at the *bottom*. A red line is drawn *under* the nucleotide sequence to represent the position of the 44 bp mini-exon. Pink peak represents the SRSF1 eCLIP signal. (*B*) Schematic of hairpin structure of miR-221 primary precursor and the 44 bp mini-exon from *MIR222HG*. Yellow box represents the mature 21 nt miR-222 position. Arrows indicate the binding sites of splicing factor SRSF1 and microprocessor (Drosha/DGCR8). (*C*) SRSF1 RIP in quiescent and 6-h serum-stimulated (SS) WI-38 cells followed by RT-qPCR to quantify the levels of *MIR222HG*, using primers detecting the 44 bp mini-exon region. (*D*) RNA stability analysis of pri-*MIR222HG* in control (gl3), Drosha-depleted, and DRCR8-depleted WI-38 cells treated by actinomycin D for indicated time points. Remaining levels of RNA are measured via RT-qPCR. (*E*) RT-qPCR to quantify the levels of spliced *MIR222HG* in control (gl3), Drosha-depleted, and DRCR8-depleted WI-38 cells. (*F*) Schematic figures showing the position of MOEs used in this study: (*a*) MOE51 and MOE53, block hairpin formation within primary miR-222, and (*b*) MOE60 blocks SRSF1 binding to the 44 bp mini-exon of *MIR222HG*. (*G*) RT-qPCR to quantify the levels of spliced *MIR222HG* in scramble and MOE-treated WI-38 cells. (*H*) RT-qPCR to quantify the levels of pre-miR-222 levels in scrambled and MOE-treated WI-38 cells, under both control (pYFP transfected) and *MIR222HG* minigene overexpressed backgrounds. (*) $P \leq 0.05$, (**) $P \leq 0.01$, (***) $P \leq 0.001$, (****) $P \leq 0.0001$ by two-tailed Student's *t*-test, $n = 3$ for all figures. Error bars represent standard deviation.

microprocessor complex (Fig. 4B). In support of this, SRSF1 RNA-IP- (RIP) followed by RT-qPCR using primers that amplify the 44 bp mini-exon region displayed enhanced association of SRSF1 to *MIR222HG* in serum-stimulated cells (Fig. 4C; Supplemental Figs. S3D, S4A). Serum-stimulated increase in the association of SRSF1 was not observed at the intronic region of *MIR222HG* (Supplemental Fig. S4Ba), nor other known SRSF1 target RNAs such as *MALAT1* lncRNA (Supplemental Fig. S4Bb), implying the specificity of the interaction. Serum-stimulated cells did not show any significant change in the cellular levels of SRSF1, indicating that differential binding of SRSF1 to *MIR222HG* mini-exon is a regulated event (Supplemental Fig. S4C). Finally, stable depletion of SRSF1 in WI-38 cells led to the skipping of the 44 bp mini-exon (Supplemental Fig. S4D,E). Based on this, we concluded that SRSF1 showed enhanced association to an exonic region within *MIR222HG*, which partially overlapped with the pri-miR-222, during serum stimulation, resulting in increased pri-*MIR222HG* splicing.

To test whether SRSF1 regulates the Drosha-mediated processing of pri-miR-222 during serum stimulation, we examined the levels of miR-222 in control and SRSF1 overexpressed or depleted WI-38 cells. To our surprise, unlike what had been reported previously in HeLa cells, both overexpression and stable depletion of SRSF1 in serum-stimulated WI-38 cells did not alter the levels of miR-222 (Supplemental Fig. S4F,G). These results argue against the earlier model that SRSF1 facilitates Drosha-mediated miR-222 synthesis (Wu et al. 2010). The disparate expression patterns of miR-221/miR-222 and spliced *MIR222HG* during serum stimulation indicate that miRNA biogenesis and splicing of *MIR222HG*, both using pri-*MIR222HG* as substrate, are regulated independently. Earlier studies have reported that, during the processing of SO-miRNA-host transcripts, differential splicing versus Drosha-mediated cleavage dictates the levels of spliced host gene transcripts versus miRNAs (Mattioli et al. 2013; Melamed et al. 2013; Agranat-Tamir et al. 2014; Pianigiani et al. 2018). In such a situation, we hypothesized that SRSF1-mediated splicing of the mini-exon in serum-stimulated cells negatively regulates the Drosha-mediated cleavage. Depletion of members of the microprocessor complex (Drosha or DRCR8) stabilized pri-*MIR222HG* and significantly increased the cellular level of spliced mature *MIR222HG* (Fig. 4D,E; Supplemental Fig. S4H,I), implying that Drosha-mediated cleavage negatively regulates the levels of mature *MIR222HG*. To further investigate the crosstalk between miR-221/222 miRNA biogenesis and *MIR222HG* splicing, we blocked the binding of

the microprocessor or SRSF1 to the pri-miR-222 hairpin or to the mini-exon, respectively, by using independent 2′-O-methoxyethyl-modified antisense oligonucleotides (MOE) (see schematic in Fig. 4F). Transfection of MOEs (MOE51 and 53) that disrupt the binding of the microprocessor robustly increased the levels of spliced *MIR222HG* (Fig. 4G). Next, we designed another MOE (MOE60) that binds to the 44 bp mini-exon of *MIR222HG* and inhibits the exon inclusion by preventing the binding of the splicing factor at the mini-exon. MOE60 transfection inhibited the inclusion of the 44 bp mini-exon of *MIR222HG*, confirming that it successfully blocked splicing factor activity (Supplemental Fig. S4J). Next, we tested whether MOE60 treatment influences miR-222 synthesis. We performed the splicing blockage experiment using MOE60 together with a *MIR222HG* minigene. Specifically, the minigene construct contained key elements of the *MIR222HG* gene (see schematic in Supplemental Fig. S4K) and could be efficiently spliced upon overexpression (data not shown). We observed that MOE60-transfected cells, which also expressed the minigene, showed a significantly increased level of pre-miR-222 (Scr vs MOE60 under minigene background, Fig. 4H), implying that reduced binding of the splicing factor at the mini-exon facilitated miR-222 synthesis. Based on these, we speculate that Drosha/DGCR8 competes with SRSF1 on the pri-*MIR222HG*, which hosts SO-miRNA miR-222. Upon serum stimulation, enhanced SRSF1 binding on pri-*MIR222HG* leads to the increased synthesis of the mature, spliced *MIR222HG*.

Spliced mature *MIR222HG* facilitates the cell cycle reentry post quiescence in a microRNA-independent manner

Increased levels of spliced *MIR222HG* in serum-stimulated cells prompted us to investigate whether it plays any role in cell cycle reentry. By transiently transducing WI-38 cells with two independent lentiviral shRNAs, we preferentially depleted the nuclear and cytoplasmic pool of only the mature spliced *MIR222HG* (Fig. 5Aa; Supplemental Fig. S5A), but not pri-*MIR222HG* (Fig. 5Ab), nor miR-222 (Fig. 5Ac). We then analyzed the ability for control or mature *MIR222HG*-depleted quiescent cells to reenter the cell cycle upon serum stimulation. PI (Propidium Iodide)-flow cytometry analyses revealed that mature *MIR222HG*-depleted cells showed a defect in cell cycle reentry, reflected by the pronounced G1 arrest and a concomitant reduction of S-phase and G2/M-phase populations (Fig. 5B). BrdU incorporation assays (45 min pulse; 24-h postserum stimulation) also revealed a reduced percentage of S-phase cells upon mature *MIR222HG*-depletion (Fig. 5C). Reduced levels of phosphorylated Retinoblastoma (pRb; S780) and Cyclin A in mature *MIR222HG*-depleted serum-stimulated cells further supported the defects in cell cycle reentry (Fig. 5D). Finally, we observed increased levels of Cyclin D1 and p27 in serum-stimulated *MIR222HG*-depleted WI-38 cells, implying that mature *MIR222HG*-depleted cells failed to enter into S-phase of the cell cycle, consistent with the reduced Cyclin A and BrdU incorporation (Fig. 5D).

To capture the changes of the transcriptome upon *MIR222HG* knockdown, we performed RNA-seq using control and mature *MIR222HG*-depleted WI-38 cells in both quiescence and 6-h serum stimulation conditions. Our analyses identified 398 genes whose expression levels were significantly altered upon knockdown by both *MIR222HG* shRNAs (Fig. 5E; Supplemental Table S6). Gene ontology analysis showed that the top biological processes, represented by those 398 genes, formed three clusters: cell proliferation, extracellular matrix organization, and cell adhesion (Fig. 5F). Pathway analysis showed that these genes were enriched in pathways including adherens, focal adhesion, Ras signaling pathway, and MAPK pathway (Supplemental Fig. S5B). All these events/pathways play crucial roles for quiescent cells to resume proliferation upon serum stimulation. Based on all these data, we concluded that the increased levels of spliced mature *MIR222HG* during serum stimulation promotes cell cycle reentry post quiescence.

Spliced *MIR222HG* depletion did not alter the levels of miR-222 (Fig. 5Ac). In addition, the levels of known canonical miR-221/222 target genes, including *CDKN1B* (p27), *KIT*, and *PTEN* (Felli et al. 2005; Cardinali et al. 2009; Chun-Zhi et al. 2010; Li et al. 2014), remained unchanged in mature *MIR222HG*-depleted cells (Supplemental Table S6). Finally, we examined the activity of miR-221/222 by performing a luciferase reporter assay using a reporter plasmid containing the 3′-UTR of the *CDKN1B* gene. We observed that the luciferase signals remained unchanged upon *MIR222HG* knockdown (Supplemental Fig. S5C), suggesting that the activity of both miRNAs were not affected. These results indicate that the cell cycle phenotype observed in *MIR222HG*-depleted cells is not due to altered levels or activity of *MIR222HG*-encoded miRNAs, implying that spliced *MIR222HG* and miR-221/222 have independent functions.

MIR222HG forms an RNP complex with ILF3/2 and other RNAs

Several lncRNAs, by interacting with proteins/RNA/DNA elements, act as a "scaffold" to modulate RNA–protein, RNA–RNA, or RNA–DNA interactions (Wang and Chang 2011; Kopp and Mendell 2018). In order to determine the molecular function of *MIR222HG* during cell cycle reentry, we investigated the *MIR222HG*-interacting proteins and RNAs. We performed streptavidin pulldown in WI-38 cell lysate using in vitro transcribed biotinylated full-length spliced *MIR222HG* or biotinylated YFP (as negative control), followed by mass spectrometry. From the protein

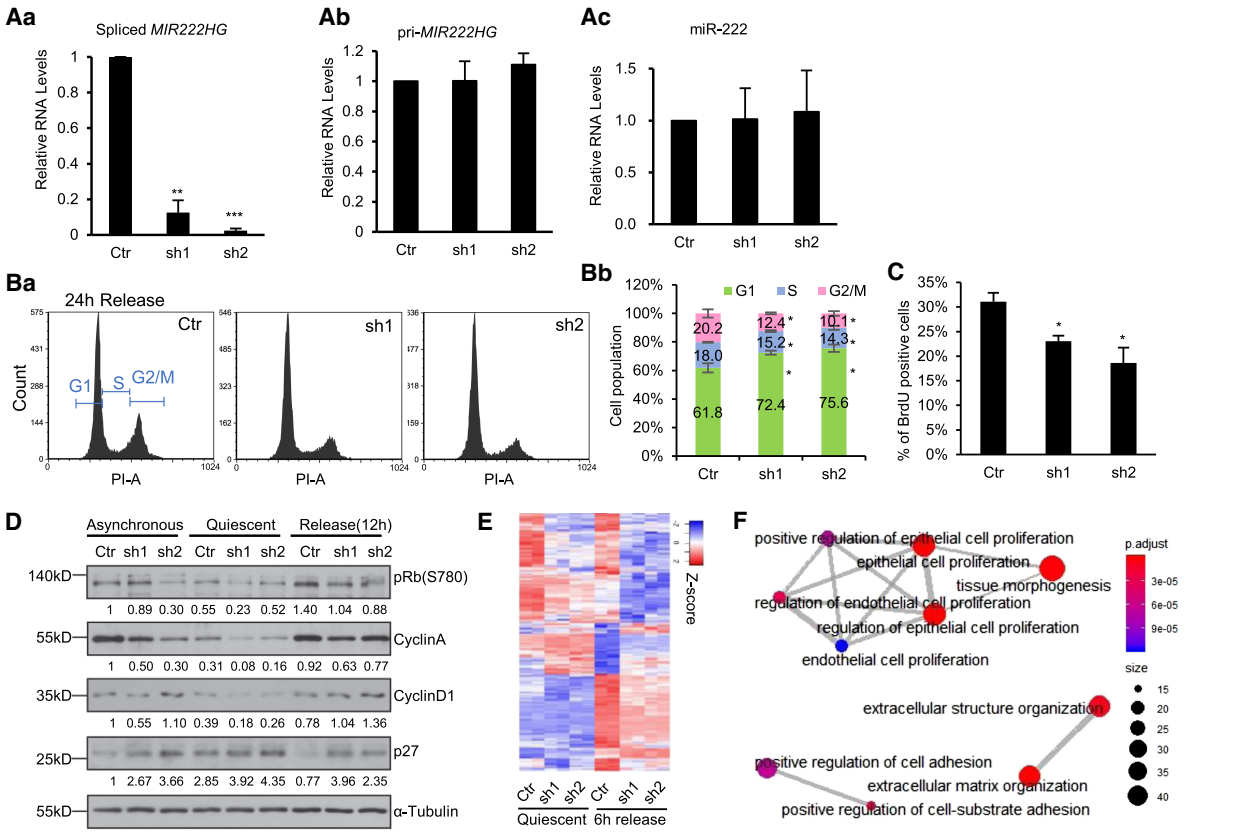

FIGURE 5. Spliced mature *MIR222HG* facilitates cell cycle reentry post quiescence in a micro-RNA independent manner. (*A*) RT-qPCR to quantify the levels of (*a*) spliced *MIR222HG*, (*b*) pri-*MIR222HG*, and (*c*) mature miR-222 (TaqMan assay), in control and *MIR222HG* shRNA treated WI-38 cells. (*B*) (*a*) PI-flow cytometry analyses in control and *MIR222HG*-depleted WI-38 cells at 24 h postserum stimulation. (*b*) Percentage of cells at a specific cell cycle stage in control and *MIR222HG*-depleted cells. Data obtained from biological triplicates. Quantification is performed using FCS Express. (*C*) Percentage of BrdU-incorporated cells in control and *MIR222HG*-depleted WI-38s at 24 h postserum stimulation. (*D*) Immunoblot to detect the levels of several cell cycle marker proteins in control and *MIR222HG*-depleted asynchronous, quiescent, and serum-stimulated (12 h) WI-38 cells. α-Tubulin is used as loading control. Quantification was performed with Image J. Relative protein levels were calculated by normalizing with GAPDH, followed by comparing to the asynchronous control sample. Values are labeled on the *bottom* of each blot. (*E*) Heatmaps showing the relative expression of 398 differentially expressed genes in control and *MIR222HG*-depleted cells during quiescence and 6-h serum stimulation, obtained by RNA-seq. Biological duplicates are represented. Genes (rows of heatmap) are hierarchically clustered using average-linkage clustering method. Detailed DEG information is available in Supplemental Table S6. (*F*) Gene ontology (GO) analyses showing the top enriched biological processes that show changes in *MIR222HG*-depleted cells. (*) $P \leq 0.05$, (**) $P \leq 0.01$, (***) $P \leq 0.001$, (****) $P \leq 0.0001$ by two-tailed Student's *t*-test, $n = 3$ for all figures. Error bars represent standard deviation.

interactome of *MIR222HG*, we identified two proteins, ILF3 (Interleukin Enhancer Binding Factor 3, or NF90) and ILF2 (Interleukin Enhancer Binding Factor 2, or NF45), as the top hits in all the three biological replicates (Supplemental Table S7). We validated the *MIR222HG*–ILF3/ILF2 interaction by immunoblotting in the biotin RNA pulldown samples (Fig. 6A). Furthermore, ILF3 RIP confirmed the interaction between endogenous ILF3 and *MIR222HG* (Fig. 6B; Supplemental Fig. S6A).

ILF3/ILF2 is an RNA-binding-protein (RBP) complex that specifically binds to double-stranded RNAs (dsRNA) and regulates RNA stabilization or translation or even ADAR-mediated A-to-I editing (Kuwano et al. 2010; Castella et al. 2015; Jiang et al. 2017; Freund et al. 2020). We examined whether *MIR222HG* forms intermolecular double stranded RNA structure with other cellular RNAs, and if such RNA–RNA structure is stabilized by the ILF3/2 complex. To test this, we performed a genome-wide bioinformatic prediction to identify RNAs that display sequence complementarity with *MIR222HG*. RNA complementarity analysis revealed that *EIF4E* mRNA and *DNM3OS* lncRNA contained multiple stretches of sequence elements that shared sequence complementarity with different regions of *MIR222HG* (Supplemental Table S8). Therefore, we performed RNA pull-down using in vitro transcribed biotinylated full-length spliced *MIR222HG* in total cell extracts and successfully validated its interaction with endogenous *EIF4E* mRNA and *DNM3OS* (Fig. 6C). Interestingly, both *EIF4E* and *DNM3OS* RNAs were previously identified as ILF3 interacting RNAs (Kuwano et al.

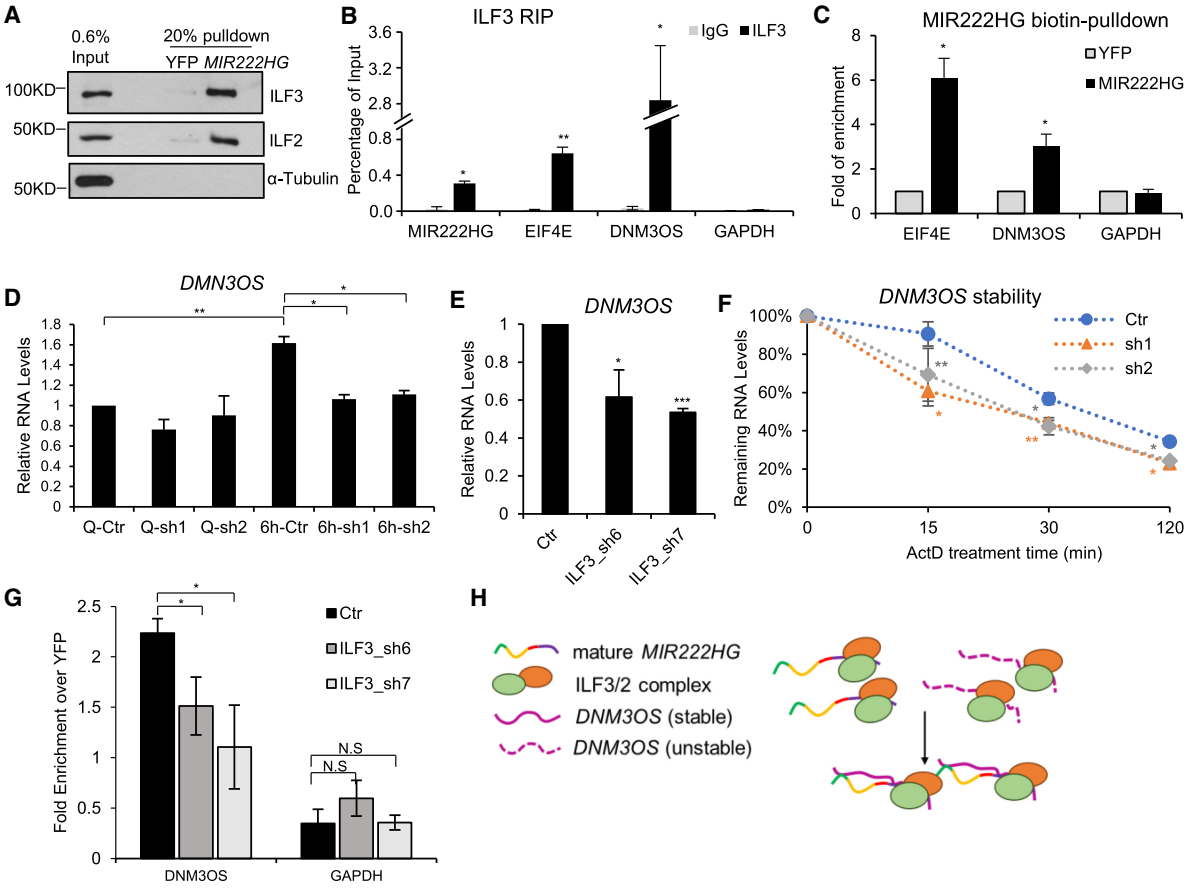

FIGURE 6. *MIR222HG* forms RNP complex containing ILF3/2 protein and other RNAs. (*A*) In vitro biotin-RNA pull-down followed by immunoblotting to detect the interaction between *MIR222HG* and ILF3/ILF2. YFP RNA is used as negative RNA control. α-Tubulin is used as negative protein control. (*B*) ILF3 RIP followed by RT-qPCR to quantify the interaction between ILF3 and *MIR222HG* or *EIF4E* (3′-UTR region) or *DNM3OS* lncRNA in WI-38 cells. *GAPDH* is used as negative control. (*C*) In vitro biotin-RNA pull-down followed by RT-qPCR to determine the interaction between *MIR222HG* and ILF3/2-target RNAs in WI-38 cells. Relative fold enrichment of *EIF4E* mRNA and *DNM3OS* lncRNA are calculated by comparing to biotin-YFP. *GAPDH* is used as negative control. (*D*) RT-qPCR to quantify the levels of *DNM3OS* lncRNA in control and *MIR222HG*-depleted WI-38 cells in quiescent and 6-h post-serum-stimulated WI-38 cells. (*E*) RT-qPCR to quantify the levels of *DNM3OS* in control and ILF3-depleted WI-38 cells post 6-h serum-stimulation. (*F*) RNA stability analyses of *DNM3OS* in control and *MIR222HG*-depleted WI-38 cells. RNA is extracted from cells incubated with actinomycin D for indicated time points (min). Relative levels of RNA are measured via RT-qPCR. (*G*) In vitro biotin-RNA pull-down followed by RT-qPCR to determine the interaction between *MIR222HG* and *DNM3OS* in control and ILF3-depleted serum-stimulated WI-38 cells. Relative fold enrichment of *DNM3OS* lncRNA is calculated by comparing to biotin-YFP. *GAPDH* is used as negative control. (*H*) Schematic of ILF3/2-*MIR222HG*-*DNM3OS* RNP complex. (*) $P \leq 0.05$, (**) $P \leq 0.01$, (***) $P \leq 0.001$, (****) $P \leq 0.0001$ by two-tailed Student's *t*-test, $n = 3$ for all figures. Error bars represent standard deviation.

2010; Das et al. 2018). We further confirmed the interaction between ILF3 and *EIF4E* and *DNM3OS* in WI-38 cells by RIP experiment (Fig. 6B). Our results indicate that *MIR222HG* along with ILF3/2 form a ribonucleoprotein (RNP) complex and interacts with several of the known ILF3/2-interacting mRNAs and lncRNAs.

We then sought to investigate whether *MIR222HG* has a role in regulating the levels or complex assembly of ILF3 and ILF2. Spliced *MIR222HG*-depleted cells did not show changes in the total cellular levels of ILF2 or both isoforms of ILF3 (NF90 and NF110) (Supplemental Fig. S6B). By performing Proximity Ligation Assay (PLA), we found that the loss of *MIR222HG* did not cause a biologically significant change in the interaction between IL3 and ILF2 (Supplemental Fig. S6C). We then investigated whether *MIR222HG* regulates the expression or stability of RNAs that interact with both *MIR222HG* and IL3/2 complex. *DNM3OS* (Dynamin-3 opposite strand) is one such candidate lncRNA that is transcribed from the intron of the *DNM3 (Dynamin-3)* gene and is conserved across mammals. *DNM3OS* is also a lnc-*MIRHG*, which encodes miR-199a-2 and miR-214. We observed that *DNM3OS* interacts with both *MIR222HG* and ILF3 (Fig. 6B,C). Our genome-wide transcriptome analyses revealed that, similar to

MIR222HG, the level of *DNM3OS* was also significantly elevated during Q to SS transition (Fig. 2F; Supplemental Table S2). RT-qPCR results also confirmed serum-stimulated induction of *DNM3OS* in WI-38 cells (Fig. 6D). Furthermore, RNA-seq as well as RT-qPCR results revealed that *MIR222HG*-depleted cells, upon serum stimulation, failed to induce *DNM3OS* levels (Fig. 6D; Supplemental Table S6). These results imply that both *MIR222HG* and *DNM3OS* are induced upon serum stimulation, and *MIR222HG* positively regulates the levels of *DNM3OS*. On the other hand, *EIF4E* mRNA and protein levels were not changed in *MIR222HG*-depleted cells (Supplemental Fig. S6B,D).

Several recent studies have reported the role of *DNM3OS* in epithelial-mesenchymal transition (EMT), cell proliferation, and inflammation, and identified *DNM3OS* as a positive regulator of cell proliferation (Watanabe et al. 2008; Mitra et al. 2017; Das et al. 2018; Ai and Yu 2019). *DNM3OS*-depleted WI-38 cells showed defects in cell cycle reentry postserum stimulation (Supplemental Fig. S6E,F), supporting its role as a mediator of pro-proliferation. Finally, *MIR222HG* depletion not only decreased *DNM3OS* levels but also reduced the level of miR-214, an exonic miRNA generated from the last exon of *DNM3OS* (Supplemental Fig. S6G). In summary, our data suggested a possibility that *MIR222HG-DNM3OS* axis could promote the cell cycle reentry of quiescent cells upon serum stimulation.

We focused our initial efforts on understanding the involvement of *MIR222HG* in regulating *DNM3OS* levels. We found that ILF3-depleted cells showed defects in the serum-stimulated induction of *DNM3OS* (Fig. 6E; Supplemental Fig. S6H). Reduced levels of *DNM3OS* in both *MIR222HG*- (Fig. 6D) and ILF3-depleted cells (Fig. 6E) suggest that ILF3/2-*MIR222HG* RNP complex could synergistically regulate the levels of *DNM3OS*. RNA stability assay showed that *DNM3OS* stability was significantly reduced upon *MIR222HG* knockdown (Fig. 6F), suggesting that *MIR222HG* facilitates the stability of *DNM3OS* RNA. We examined whether *MIR222HG* regulates *DNM3OS* stability by modulating the interaction between ILF3 and *DNM3OS*. Control and *MIR222HG*-depleted cells did not show any significant difference in the interaction between ILF3 and *DNM3OS*, as observed by ILF3 RIP followed by RT-qPCR (Supplemental Fig. S6I). Next, we asked whether the ILF3/2 complex facilitates the interaction between *MIR222HG* and *DNM3OS*. *MIR222HG* biotin-RNA pull-down followed by RT-qPCR in control and ILF3-depleted serum-stimulated cell extracts revealed reduced interactions between *MIR222HG* and *DNM3OS* upon ILF3 depletion (Fig. 6G). Based on our results, we speculate that during serum stimulation, *MIR222HG* along with IL3/2 form an RNP complex to stabilize *DNM3OS* (Fig. 6H), thereby promoting cell cycle reentry post cellular quiescence.

DISCUSSION

In the present study, we focus on understanding the role of lncRNAs during cell cycle reentry. Within the lncRNA repertoire, lnc-*MIRHG*s (*microRNA-host-gene* lncRNAs) constitute an understudied family because they are often considered as primary miRNA transcripts, without additional functions. In support of this argument, studies have reported that several pri-*MIRHGs* are cleaved by Drosha to make unproductive transcripts (Dhir et al. 2015a; Pianigiani et al. 2018). However, earlier independent studies from our laboratory as well as other groups have documented miRNA-independent roles of lnc-*MIRHG*s (Ng et al. 2013; Tseng et al. 2014; Colombo et al. 2015; Raveh et al. 2015; Shih et al. 2017; Sun et al. 2018b; Du et al. 2019; Profumo et al. 2019). In the present study, we systematically annotated the role of human *MIR222HG* in cell cycle reentry. These examples strongly support the idea that it is not an uncommon but a rather general genomic mechanism for a single gene locus to generate two classes of independently functional noncoding RNAs.

From our RNA-seq analyses, we identified several differentially expressed lnc-*MIRHG*s (DE-lnc-*MIRHG*s) during the course of quiescence onset and cell cycle reentry. The up-regulated DE-lnc-*MIRHG*s during serum stimulation have the potential to facilitate the quiescence exit/cell cycle reentry, which is an event strongly associated with tumor reoccurrence. Hence, it is not surprising that some of the up-regulated DE-lnc-*MIRHG*s that we identified in our study (*MIR31HG*, *MIR22HG*, and *MIR17HG)* were previously recognized as cancer biomarkers or regulators of cancer progression (Montes et al. 2015; Shih et al. 2017; Su et al. 2018; Xu et al. 2019; Yuan et al. 2019). For instance, *MIR17HG* can promote tumorigenesis and metastasis of colorectal cancer and gastric cancer (Xu et al. 2019; Yuan et al. 2019). *MIR31HG* has been shown to play roles in senescence modulation (Montes et al. 2015), *MIR31HG* has also been shown to play miR-31-independent functions in regulating the HIF-1 transcriptional network to drive oral cancer progression (Shih et al. 2017). These studies have substantiated the biological significance of the DE-lnc-*MIRHG*s identified in our study.

Previous studies have reported coregulated or independent expression patterns of miRNAs and their host genes (Baskerville and Bartel 2005; Lutter et al. 2010; Budach et al. 2016; Liu et al. 2018; Steiman-Shimony et al. 2018). For example, *DLEU2*, which is down-regulated in pediatric acute myeloid leukemia, was shown to express independently from miR-15a/16-1, which are encoded within *DLEU2* (Morenos et al. 2014). Also, we previously demonstrated that *MIR100HG* was up-regulated in G1 phase of the cell cycle, independently of its encoded miRNAs, such as miR-100 (Sun et al. 2018b). Similarly, in the present study, we showed that spliced *MIR222HG*, but not miR-221 or miR-222, was dramatically up-regulated during

serum stimulation, implying that the mature *MIR222HG* and miR-221/222 display independent expression patterns. We also demonstrated that the major inciting factor for the induction of mature *MIR222HG* upon serum stimulation was the increased splicing efficiency of pri-*MIR222HG*, due to enhanced SRSF1 binding. Our findings suggest that transcriptional and posttranscriptional regulations cooperate to fine-tune the levels of mature lnc-*MIRHG*s and the miRNAs that are encoded within the *MIRHGs*. It is not yet known how the association of SRSF1 to *MIR222HG* is being regulated. We speculate that SRSF1 binding could be modulated by serum-induced posttranslational modifications of SRSF1 (i.e., phosphorylation). Alternatively, serum induction probably could promote the recruitment of SRSF1-interacting factors to *MIR222HG*, which stabilizes the association of SRSF1 to the *MIR222HG* transcript.

During the processing of SO-miRNAs, the crosstalk between the splicing factors and microprocessor proteins dictates the relationship between miRNA biogenesis and host gene RNA splicing. This falls under two general models: "synergic" and "competitive," as described by several previous studies (Wu et al. 2010; Janas et al. 2011; Westholm and Lai 2011; Mattioli et al. 2013, 2014; Melamed et al. 2013; Agranat-Tamir et al. 2014; Pianigiani et al. 2018). Synergic cases are exemplified by a type of intronic miRNAs "mirtrons" whose production depends on the splicing of their host gene (Berezikov et al. 2007b; Westholm and Lai 2011). On the other hand, *MCM7* and *MIR202HG*, which host miR-106b-25 and miR-202, respectively, identify examples of the competitive model (Melamed et al. 2013; Agranat-Tamir et al. 2014). Notably, both miR-106b-25 and miR-202 are splice site overlapping miRNAs (SO-miRNAs) (Mattioli et al. 2014). We defined miR-222 as a SO-miRNA in light of the newly identified 44 bp mini-exon that partially overlaps with pri-miR-222. We concluded that the splicing and microprocessor machinery compete to process the pri-*MIR222HG* transcripts during serum stimulation, reflected by the observation that Drosha/DGCR8 complex antagonizes the access of SRSF1 to pri-*MIR222HG*. In this context, an earlier study reported that SRSF1, instead of playing its canonical role as a splicing factor, facilitated Drosha-mediated processing of pre-miRNAs (Wu et al. 2010). The authors reported that the overexpression of SRSF1 in HeLa cells caused increased levels of several miRNAs, including miR-7, miR-221, and miR-222. In addition to the mature miRNA levels, SRSF1 overexpression also increased the levels of pre-miRNAs when cells expressed minigenes containing miRNA precursors. Based on this, the authors claimed that SRSF1 promotes the Drosha cleavage step of pri-miRNA processing, resulting in enhanced syntheses of multiple miRNAs, including miR-222/221. However, in WI-38 diploid fibroblasts, overexpression or knockdown of SRSF1 did not affect the levels of miR-222. One possible explanation for the discrepancy in results could be the fact that the two studies utilized different cell lines and physiological conditions (serum-stimulated WI-38 diploid fibroblasts versus asynchronous HeLa cancer cell line). LncRNA genes are shown to generate a variety of isoforms in different cell lines/tissues/species/biological scenarios (Ziegler and Kretz 2017). We speculate that Hela cells might not express the serum-responsive *MIR222HG* isoform that contains the 44 bp mini-exon. In such a scenario, miR-222 would behave as an intronic miRNA and could rely on splicing for its biogenesis. In summary, these observations indicate that *MIR222HG* gene expression is regulated by differential splicing and intragenic miRNA biogenesis in a cell type-specific manner.

LncRNAs can modulate transcription, pre-mRNA splicing, RNA stability, and protein translation by regulating the recruitment of proteins to chromatin and/or RNA (Wang and Chang 2011; Noh et al. 2018; Sun et al. 2018a; He et al. 2019). We found that spliced *MIR222HG* associated with the ILF3/2 complex. ILF3/2 heterodimeric protein complex regulates both transcription and posttranscriptional events, such as RNA stability and translation (Kuwano et al. 2010; Hu et al. 2013; Castella et al. 2015; Nakadai et al. 2015; Jiang et al. 2017; Wu et al. 2018). Earlier studies demonstrated the involvement of the ILF3/2 complex in modulating lncRNA functions. For example, lncRNA *LincIN*-ILF3 complex regulates breast cancer metastasis by inhibiting p21 translation (Jiang et al. 2017), and ILF3-*SALNR* lncRNA complex modulates miRNA biogenesis (Wu et al. 2015). Our data indicated that *MIR222HG*, *DNM3OS*, and ILF3/2 form RNP complex, and *MIR222HG*/ILF3 complex positively regulate the stability of *DNM3OS* lncRNA. Furthermore, we demonstrated that ILF3/2-facilitates the interaction between *MIR222HG* and *DNM3OS*. Hence, we hypothesize that ILF3/2, with their inherent ability to bind to double-stranded RNAs, act as a "scaffold" to promote *MIR222HG-DNM3OS* duplex formation, and thereby stabilize *DNM3OS*. A similar mechanism has been previously identified in the case of *HOTAIR*-hnRNP B1 complex (Meredith et al. 2016; Nguyen et al. 2018). HnRNP B1, by forming an RNP-complex with *HOTAIR* facilitates RNA–RNA interactions between *HOTAIR* and several target RNAs to initiate the heterochromatinization. We therefore speculate that, ILF3, like hnRNP B1, functions as an "RNA matchmaker protein."

We found that *DNM3OS*-depleted WI-38 cells displayed defects in cell proliferation post quiescence, which suggests that *DNM3OS* could be one of the downstream effectors of *MIR222HG*–ILF3/2 axis. *DNM3OS* has been previously shown to be involved in cell growth/proliferation (Watanabe et al. 2008; Mitra et al. 2017; Ai and Yu 2019). In human chondrocyte cells, *DNM3OS* enhanced cell proliferation (Ai and Yu 2019). In mice, *DNM3OS* was found to be essential for normal growth, based on a study that showed its depletion caused defects in birth and/or

development (Watanabe et al. 2008). *DNM3OS* is also known to facilitate the mesenchymal-to-epithelial transition, cancer cell migration, and invasion; and elevated levels of *DNM3OS* in patients were associated with poor survival (Mitra et al. 2017). In this particular study, the authors have reported that depletion of *DNM3OS* altered multiple pathways including cytoskeleton regulation, adherens junction, focal adhesion, and MAPK signaling pathways. Interestingly, *MIR222HG*-depleted cells also displayed defects in similar events/pathways (Fig. 5F; Supplemental Fig. S5B), implying the involvement of *MIR222HG-DNM3OS* axis in influencing crucial pathways that regulate cell cycle reentry. Based on this, we speculate that *MIR222HG* depletion caused cell cycle defects by reducing the cellular level of another pro-proliferative lnc-*MIRHG, DNM3OS*. Future studies will focus on the molecular mechanism by which *MIR222HG* controls *DNM3OS* activity.

Although, in the current study, we identified the involvement of *MIR222HG*–ILF3 RNP complex in regulating the RNA stability of *DNM3OS*, a cell cycle regulator, we cannot rule out the possibility that *MIR222HG*–ILF3 could in addition engage in other molecular processes. For example, ILF3 has been shown, by multiple studies, to have pro-proliferative roles by serving as transcription factor or cofactor to facilitate the expression of early serum-responsive genes, including *EGR1*, *MYC*, *JUN*, and *FOS* (Nakadai et al. 2015; Wu et al. 2018, 2019). Hence, it might also be possible that *MIR222HG* plays additional roles in regulating transcription via modulating ILF3/ILF2 transcription factor/cofactor activity.

We have proposed a working model to summarize our findings about how *MIR222HG* promotes cell cycle reentry post quiescence (Fig. 7). We showed that the abundant and unstable pri-*MIR222HG* could undergo two mutually independent processes. The dominant role of pri-*MIR222HG* is to act as a substrate for miR-221/222 biogenesis. However, upon serum stimulation, a small but significant fraction of pri-*MIR222HG* undergoes splicing, which is mediated by enhanced SRSF1 binding, resulting in elevated levels of the spliced mature *MIR222HG* lncRNA. The mature lncRNA *MIR222HG* exerts miRNA-independent functions to facilitate cell cycle reentry. Our preliminary studies support a model that *MIR222HG*–ILF3/2 axis assures the success of cell cycle reentry in WI-38 cells.

MATERIALS AND METHODS

Cell culture

WI-38 cells were cultured in 10% FBS + MEM with nonessential amino acids (NEAA) and sodium pyruvate. To induce cellular quiescence, cells were cultured in 0.1% serum for 3 d. Then, serum reactivation was performed by adding back the regular 10% serum growth medium. For lentivirus packaging, HEK293T cells were cultured using DMEM containing 10%FBS (heat inactivated).

RNA-seq and bioinformatics analyses

Total RNA was extracted using RNeasy Mini Kit and DNA was removed using DNase I (Qiagen, Cat# 74104). The RNA-seq libraries were prepared with Illumina's TruSeq Stranded mRNAseq Sample Prep kit and polyadenylated mRNAs were captured with oligo(dT) beads. Paired-end, poly(A)$^+$ RNA-sequencing was performed on the Illumina platform (Novaseq 6000, SP flowcell) at the Roy J. Carver Biotechnology Center at UIUC. Quality of RNA-seq reads was examined by FASTQC. RNA-seq reads were aligned to the human reference genome GRCh38 assembly using HISAT2 (Kim et al. 2015). Transcript assembly and expression assessment was performed using Stringtie (Pertea et al. 2015) to get the TPM (Transcripts Per Million) values for each gene. Read coverage BigWig (bw) files were generated with RPKM normalization using bamCoverage in deepTools (Ramirez et al. 2016). Bw files from two biological replicates were further merged using bigWigMerge and bedGraghToBigWig. For statistical analyses, raw gene counts were first analyzed by HTseq-Count (Anders et al. 2015), then analyzed using edgeR (Robinson et al. 2010).

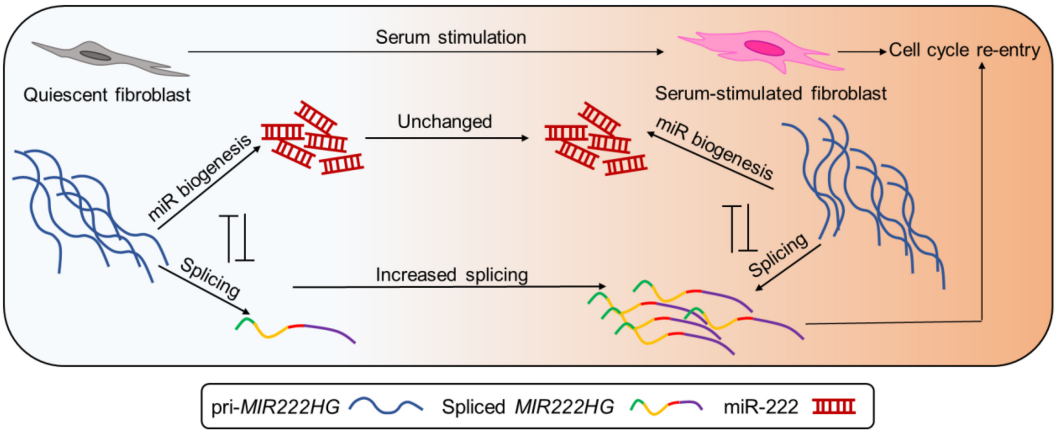

FIGURE 7. Schematic of *MIR222HG* biogenesis and potential mode of action.

Qualifiable expression was defined by CPM ≥ 0.1 in at least two samples out of total eight samples. Normalization of library size was performed by calcNormFactors in edgeR with the default TMM method. For visualization of the transcriptome profile, heatmaps were plotted using coolmap function from limma package (Ritchie et al. 2015), with row centering and scaling. Hierarchical clustering of genes (rows) was performed with average-linkage method. Differential expression analyses were performed using exactTest between every two adjacent cell cycle phases. Differentially expressed genes (DEGs) were defined by $|\log_2(\text{fold change})| > 1$ and FDR < 0.05.

Gene ontology analyses and GSEA (gene set enrichment analysis) were performed using clusterProfiler of Bioconductor (Yu et al. 2012). Specifically, gene ontology for biological process was performed using enrichGO function, Kegg pathway analyses were performed using enrichKEGG. All enrichment analyses include using a background gene list containing all 17,640 genes that showed qualifiable expression in the RNA-seq. GSEA analysis was performed using gseGO function and gene lists were ranked using $\log F_C$ values.

*MIRHG*s, in this study, were defined when the coordinates of a gene include the coordinates of a miRNA gene. The coordinate information of the gene/exons was extracted from the GRCh38 assembly GTF file (v94 of Ensembl). For intragenic miRNA categorization, miRNAs that completely locate within any exon of a *MIRHG* were defined as exonic-miRs. MiRs were defined as intronic miRs when they do not overlap with any exonic regions of any genes. The rest of intragenic miRNAs were then defined as spliced site overlapping miRNAs (SO-miRs).

MicroRNA quantification

TaqMan assays were performed for measuring the mature miRNAs as per manufacturer's instruction. hsa-miR-222 was measured and normalized to U6 (TaqMan, Cat# 4427975 with AssayID 002276 and 001973, respectively). The method of measuring precursor miRNA (pre-miRs) was adapted from a previous study (Kawahara 2012). Small RNAs were isolated using miRVANA (Ambion, Cat# AM1560). 1ug small RNA was then used for 3′ Polyadenylation addition using Poly(A) Polymerase Tailing Kit (Epicentre, Cat# PAP5104H), followed by DNase I treatment (Sigma, Cat# AMPD1) and reverse transcription (Applied Biosystems, Cat# 4368814) with a customized RT primer (Customized Oligo-dT RT primer, see primer table in Supplemental Materials and Methods). Quantification of pre-miRNAs was performed by RT-qPCR with customized primers (222-3tail-qPCR-F, U6-3tail-qPCR-F, 3tail-qpcr-R, see primer table in Supplemental Materials and Methods). U6 served as loading control.

Single-molecule fluorescence RNA in situ hybridization (smRNA-FISH)

The *MIR222HG* smRNA FISH probe set was designed using Stellaris Probe Designer, and consisted of 29 20-mer DNA oligonucleotides. Full-length (1.3 kb) *MIR222HG* sequence was used as input for probe design. 3′amino group modified oligonucleotides (LGC Biosearch Technologies) were pooled and coupled with Cy3 Mono NHS Ester (GE Healthcare). WI-38 cells were seeded on coverslips for serum starvation and release. At harvest, cells were fixed with 10% neutral buffered formalin (Sigma, HT501128) for 10 min at room temperature and permeabilized with 70% ethanol for overnight at −20°C. The coverslips were then washed with Buffer A (20% Stellaris RNA FISH Wash Buffer A [Biosearch Technologies, SMF-WA1-60] and 10% formamide in nuclease-free water) for 5 min at room temperature and incubated with hybridization buffer (90% Stellaris RNA FISH Hybridization Buffer [Biosearch Technologies, SMF-HB1-10] and 10% formamide) containing ∼125 nM of the Cy3-labeled *MIR222HG* smFISH probe in a humidified chamber in the dark at 37°C for 16 h. After hybridization, the coverslips were washed twice with Buffer A, 30 min for each of the washes, in the dark at 37°C. DNA were counterstained by DAPI during the second wash. The coverslips were then washed with Stellaris RNA FISH Wash Buffer B (Biosearch Technologies, SMF-WB1-20) for 5 min in the dark at room temperature and mounted onto microscope slides with VectaShield Antifade Mounting Medium (Vector Laboratories, H-1000). Z-stack images were taken using DeltaVision microscope (GE) equipped with 60×/1.42 NA oil immersion objective (Olympus) and CoolSNAP-HQ2 camera. Images were then processed through deconvolution and maximum intensity projection.

DATA DEPOSITION

RNA-seq files were submitted to GEO. The asynchronous, quiescent, and serum stimulated WI-38 RNA-seq files are in GSE144710. The RNA-seq data of *MIR222HG*-depletion experiment are in GSE145212. Mass spectrometric data has been submitted to ProteomeXchange via the PRIDE database (PXD017585).

SUPPLEMENTAL MATERIAL

Supplemental material is available for this article.

COMPETING INTEREST STATEMENT

S.M.F. is an employee of Ionis Inc. and receives a salary from Ionis Inc.

ACKNOWLEDGMENTS

We would like to thank K.V. Prasanth and S.G. Prasanth laboratory members for their comments and suggestions. We thank Dr. Brian Freeman (UIUC) for sharing equipment and Dr. Alvaro Hernandez (J. Carver Biotechnology Center Directory, UIUC) for technical support for RNA-seq. We also thank the CCR, National Institutes of Health (NIH) sequencing core for help with RNA-seq. Work in the K.V.P. laboratory was supported by grants from the National Institute on Aging/NIH (R21AG065748), Cancer Center at Illinois seed grant, Prairie Dragon Paddlers, and the National Science Foundation (NSF) (EAGER; MCB1723008). Work in the S.G.P. laboratory is supported by the NSF (1243372 and 1818286) and the NIH (GM125196). Work in the A.K. laboratory is supported by the NIH (R01HL126845, R01AA010154), Muscular Dystrophy Association (MDA514335), Planning Grant Award from the Cancer Center at Illinois, and a Beckman Fellowship from the Center for Advanced Study at the University of Illinois Urbana-

Champaign. S.B. is supported by the NIH Tissue Microenvironment Training Program (T32-EB019944). J.-H.C. and J.-H.Y were funded by the Medical University of South Carolina.

Received March 5, 2020; accepted July 8, 2020.

REFERENCES

Agranat-Tamir L, Shomron N, Sperling J, Sperling R. 2014. Interplay between pre-mRNA splicing and microRNA biogenesis within the supraspliceosome. *Nucleic Acids Res* **42:** 4640–4651. doi:10.1093/nar/gkt1413

Ai D, Yu F. 2019. LncRNA DNM3OS promotes proliferation and inhibits apoptosis through modulating IGF1 expression by sponging MiR-126 in CHON-001 cells. *Diagn Pathol* **14:** 106. doi:10.1186/s13000-019-0877-2

Ameres SL, Zamore PD. 2013. Diversifying microRNA sequence and function. *Nat Rev Mol Cell Biol* **14:** 475–488. doi:10.1038/nrm3611

Anders S, Pyl PT, Huber W. 2015. HTSeq–a Python framework to work with high-throughput sequencing data. *Bioinformatics* **31:** 166–169. doi:10.1093/bioinformatics/btu638

Augoff K, McCue B, Plow EF, Sossey-Alaoui K. 2012. miR-31 and its host gene lncRNA LOC554202 are regulated by promoter hypermethylation in triple-negative breast cancer. *Mol Cancer* **11:** 5. doi:10.1186/1476-4598-11-5

Bainbridge P. 2013. Wound healing and the role of fibroblasts. *J Wound Care* **22:** 407–408. doi:10.12968/jowc.2013.22.8.407

Baskerville S, Bartel DP. 2005. Microarray profiling of microRNAs reveals frequent coexpression with neighboring miRNAs and host genes. *RNA* **11:** 241–247. doi:10.1261/rna.7240905

Berezikov E, Chung WJ, Willis J, Cuppen E, Lai EC. 2007a. Mammalian mirtron genes. *Mol Cell* **28:** 328–336. doi:10.1016/j.molcel.2007.09.028

Berezikov E, Chung WJ, Willis J, Cuppen E, Lai EC. 2007b. Mammalian mirtron genes. *Mol Cell* **28:** 328–336. doi:10.1016/j.molcel.2007.09.028

Bierhoff H, Dammert MA, Brocks D, Dambacher S, Schotta G, Grummt I. 2014. Quiescence-induced lncRNAs trigger H4K20 trimethylation and transcriptional silencing. *Mol Cell* **54:** 675–682. doi:10.1016/j.molcel.2014.03.032

Budach S, Heinig M, Marsico A. 2016. Principles of microRNA regulation revealed through modeling microRNA expression quantitative trait loci. *Genetics* **203:** 1629–1640.

Busch A, Hertel KJ. 2012. Evolution of SR protein and hnRNP splicing regulatory factors. *Wiley Interdiscip Rev RNA* **3:** 1–12.

Cardinali B, Castellani L, Fasanaro P, Basso A, Alema S, Martelli F, Falcone G. 2009. MicroRNA-221 and microRNA-222 modulate differentiation and maturation of skeletal muscle cells. *PLoS ONE* **4:** e7607. doi:10.1371/journal.pone.0007607

Castella S, Bernard R, Corno M, Fradin A, Larcher JC. 2015. Ilf3 and NF90 functions in RNA biology. *Wiley Interdiscip Rev RNA* **6:** 243–256. doi:10.1002/wrna.1270

Chen YG, Satpathy AT, Chang HY. 2017. Gene regulation in the immune system by long noncoding RNAs. *Nat Immunol* **18:** 962–972. doi:10.1038/ni.3771

Cheung TH, Rando TA. 2013. Molecular regulation of stem cell quiescence. *Nat Rev Mol Cell Biol* **14:** 329–340. doi:10.1038/nrm3591

Cheung TH, Quach NL, Charville GW, Liu L, Park L, Edalati A, Yoo B, Hoang P, Rando TA. 2012. Maintenance of muscle stem-cell quiescence by microRNA-489. *Nature* **482:** 524–528. doi:10.1038/nature10834

Choi SW, Kim HW, Nam JW. 2019. The small peptide world in long noncoding RNAs. *Brief Bioinformatics* **20:** 1853–1864. doi:10.1093/bib/bby055

Chun-Zhi Z, Lei H, An-Ling Z, Yan-Chao F, Xiao Y, Guang-Xiu W, Zhi-Fan J, Pei-Yu P, Qing-Yu Z, Chun-Sheng K. 2010. MicroRNA-221 and microRNA-222 regulate gastric carcinoma cell proliferation and radioresistance by targeting PTEN. *BMC Cancer* **10:** 367. doi:10.1186/1471-2407-10-367

Coller HA. 2007. What's taking so long? S-phase entry from quiescence versus proliferation. *Nat Rev Mol Cell Biol* **8:** 667–670. doi:10.1038/nrm2223

Coller HA. 2011. Cell biology. The essence of quiescence. *Science* **334:** 1074–1075. doi:10.1126/science.1216242

Coller HA, Sang L, Roberts JM. 2006. A new description of cellular quiescence. *PLoS Biol* **4:** e83. doi:10.1371/journal.pbio.0040083

Colombo T, Farina L, Macino G, Paci P. 2015. PVT1: a rising star among oncogenic long noncoding RNAs. *Biomed Res Int* **2015:** 304208. doi:10.1155/2015/304208

Das S, Reddy MA, Senapati P, Stapleton K, Lanting L, Wang M, Amaram V, Ganguly R, Zhang L, Devaraj S, et al. 2018. Diabetes mellitus-induced long noncoding RNA *Dnm3os* regulates macrophage functions and inflammation via nuclear mechanisms. *Arterioscler Thromb Vasc Biol* **38:** 1806–1820. doi:10.1161/ATVBAHA.117.310663

Dhir A, Dhir S, Proudfoot NJ, Jopling CL. 2015a. Microprocessor mediates transcriptional termination of long noncoding RNA transcripts hosting microRNAs. *Nat Struct Mol Biol* **22:** 319–327. doi:10.1038/nsmb.2982

Dhir A, Dhir S, Proudfoot NJ, Jopling CL. 2015b. Microprocessor mediates transcriptional termination of long noncoding RNA transcripts hosting microRNAs. *Nat Struct Mol Biol* **22:** 319–327. doi:10.1038/nsmb.2982

Du Q, Hoover AR, Dozmorov I, Raj P, Khan S, Molina E, Chang TC, de la Morena MT, Cleaver OB, Mendell JT, et al. 2019. *MIR205HG* is a long noncoding RNA that regulates growth hormone and prolactin production in the anterior pituitary. *Dev Cell* **49:** 618–631 e615. doi:10.1016/j.devcel.2019.03.012

Fang Y, Fullwood MJ. 2016. Roles, functions, and mechanisms of long non-coding RNAs in cancer. *Genomics Proteomics Bioinformatics* **14:** 42–54. doi:10.1016/j.gpb.2015.09.006

Felli N, Fontana L, Pelosi E, Botta R, Bonci D, Facchiano F, Liuzzi F, Lulli V, Morsilli O, Santoro S, et al. 2005. MicroRNAs 221 and 222 inhibit normal erythropoiesis and erythroleukemic cell growth via kit receptor down-modulation. *Proc Natl Acad Sci* **102:** 18081–18086. doi:10.1073/pnas.0506216102

Flynn RA, Chang HY. 2014. Long noncoding RNAs in cell-fate programming and reprogramming. *Cell Stem Cell* **14:** 752–761. doi:10.1016/j.stem.2014.05.014

Freund EC, Sapiro AL, Li Q, Linder S, Moresco JJ, Yates JR III, Li JB. 2020. Unbiased identification of *trans* regulators of ADAR and A-to-I RNA editing. *Cell Rep* **31:** 107656. doi:10.1016/j.celrep.2020.107656

Garofalo M, Quintavalle C, Romano G, Croce CM, Condorelli G. 2012. miR221/222 in cancer: their role in tumor progression and response to therapy. *Curr Mol Med* **12:** 27–33. doi:10.2174/156652412798376170

Gos M, Miloszewska J, Swoboda P, Trembacz H, Skierski J, Janik P. 2005. Cellular quiescence induced by contact inhibition or serum withdrawal in C3H10T1/2 cells. *Cell Prolif* **38:** 107–116. doi:10.1111/j.1365-2184.2005.00334.x

Harashima H, Dissmeyer N, Schnittger A. 2013. Cell cycle control across the eukaryotic kingdom. *Trends Cell Biol* **23:** 345–356. doi:10.1016/j.tcb.2013.03.002

He RZ, Luo DX, Mo YY. 2019. Emerging roles of lncRNAs in the post-transcriptional regulation in cancer. *Genes Dis* **6:** 6–15. doi:10.1016/j.gendis.2019.01.003

Hu Q, Lu YY, Noh H, Hong S, Dong Z, Ding HF, Su SB, Huang S. 2013. Interleukin enhancer-binding factor 3 promotes breast tumor

progression by regulating sustained urokinase-type plasminogen activator expression. *Oncogene* **32:** 3933–3943. doi:10.1038/onc.2012.414

Janas MM, Khaled M, Schubert S, Bernstein JG, Golan D, Veguilla RA, Fisher DE, Shomron N, Levy C, Novina CD. 2011. Feed-forward microprocessing and splicing activities at a microRNA-containing intron. *PLoS Genet* **7:** e1002330. doi:10.1371/journal.pgen.1002330

Jiang Z, Slater CM, Zhou Y, Devarajan K, Ruth KJ, Li Y, Cai KQ, Daly M, Chen X. 2017. LincIN, a novel NF90-binding long non-coding RNA, is overexpressed in advanced breast tumors and involved in metastasis. *Breast Cancer Res* **19:** 62. doi:10.1186/s13058-017-0853-2

Kahl G. 2009. *The dictionary of genomics, transcriptomics and proteomics.* Wiley-Blackwell, Hoboken, NJ.

Kato M, Wang M, Chen Z, Bhatt K, Oh HJ, Lanting L, Deshpande S, Jia Y, Lai JY, O'Connor CL, et al. 2016. An endoplasmic reticulum stress-regulated lncRNA hosting a microRNA megacluster induces early features of diabetic nephropathy. *Nat Commun* **7:** 12864. doi:10.1038/ncomms12864

Kawahara Y. 2012. Quantification of adenosine-to-inosine editing of microRNAs using a conventional method. *Nat Protoc* **7:** 1426–1437. doi:10.1038/nprot.2012.073

Kim D, Langmead B, Salzberg SL. 2015. HISAT: a fast spliced aligner with low memory requirements. *Nat Methods* **12:** 357–360. doi:10.1038/nmeth.3317

Kitagawa M, Kitagawa K, Kotake Y, Niida H, Ohhata T. 2013. Cell cycle regulation by long non-coding RNAs. *Cell Mol Life Sci* **70:** 4785–4794. doi:10.1007/s00018-013-1423-0

Kopp F, Mendell JT. 2018. Functional classification and experimental dissection of long noncoding RNAs. *Cell* **172:** 393–407. doi:10.1016/j.cell.2018.01.011

Kuwano Y, Pullmann R Jr, Marasa BS, Abdelmohsen K, Lee EK, Yang X, Martindale JL, Zhan M, Gorospe M. 2010. NF90 selectively represses the translation of target mRNAs bearing an AU-rich signature motif. *Nucleic Acids Res* **38:** 225–238. doi:10.1093/nar/gkp861

Laporte D, Lebaudy A, Sahin A, Pinson B, Ceschin J, Daignan-Fornier B, Sagot I. 2011. Metabolic status rather than cell cycle signals control quiescence entry and exit. *J Cell Biol* **192:** 949–957. doi:10.1083/jcb.201009028

Lemons JM, Feng XJ, Bennett BD, Legesse-Miller A, Johnson EL, Raitman I, Pollina EA, Rabitz HA, Rabinowitz JD, Coller HA. 2010. Quiescent fibroblasts exhibit high metabolic activity. *PLoS Biol* **8:** e1000514. doi:10.1371/journal.pbio.1000514

Li Y, Liang C, Ma H, Zhao Q, Lu Y, Xiang Z, Li L, Qin J, Chen Y, Cho WC, et al. 2014. miR-221/222 promotes S-phase entry and cellular migration in control of basal-like breast cancer. *Molecules* **19:** 7122–7137. doi:10.3390/molecules19067122

Li J, Tian H, Yang J, Gong Z. 2016. Long noncoding RNAs regulate cell growth, proliferation, and apoptosis. *DNA Cell Biol* **35:** 459–470. doi:10.1089/dna.2015.3187

Liu H, Adler AS, Segal E, Chang HY. 2007. A transcriptional program mediating entry into cellular quiescence. *PLoS Genet* **3:** e91. doi:10.1371/journal.pgen.0030091

Liu B, Shyr Y, Cai J, Liu Q. 2018. Interplay between miRNAs and host genes and their role in cancer. *Brief Funct Genomics* **18:** 255–266. doi:10.1093/bfgp/elz002

Lutter D, Marr C, Krumsiek J, Lang EW, Theis FJ. 2010. Intronic microRNAs support their host genes by mediating synergistic and antagonistic regulatory effects. *BMC Genomics* **11:** 224. doi:10.1186/1471-2164-11-224

Marchese FP, Raimondi I, Huarte M. 2017. The multidimensional mechanisms of long noncoding RNA function. *Genome Biol* **18:** 206. doi:10.1186/s13059-017-1348-2

Martinez I, Hayes KE, Barr JA, Harold AD, Xie M, Bukhari SIA, Vasudevan S, Steitz JA, DiMaio D. 2017. An Exportin-1-dependent microRNA biogenesis pathway during human cell quiescence. *Proc Natl Acad Sci* **114:** E4961–E4970. doi:10.1073/pnas.1618732114

Mattioli C, Pianigiani G, Pagani F. 2013. A competitive regulatory mechanism discriminates between juxtaposed splice sites and pri-miRNA structures. *Nucleic Acids Res* **41:** 8680–8691. doi:10.1093/nar/gkt614

Mattioli C, Pianigiani G, Pagani F. 2014. Cross talk between spliceosome and microprocessor defines the fate of pre-mRNA. *Wiley Interdiscip Rev RNA* **5:** 647–658. doi:10.1002/wrna.1236

Mayoral RJ, Deho L, Rusca N, Bartonicek N, Saini HK, Enright AJ, Monticelli S. 2011. MiR-221 influences effector functions and actin cytoskeleton in mast cells. *PLoS ONE* **6:** e26133. doi:10.1371/journal.pone.0026133

Medina R, Zaidi SK, Liu CG, Stein JL, van Wijnen AJ, Croce CM, Stein GS. 2008. MicroRNAs 221 and 222 bypass quiescence and compromise cell survival. *Cancer Res* **68:** 2773–2780. doi:10.1158/0008-5472.CAN-07-6754

Melamed Z, Levy A, Ashwal-Fluss R, Lev-Maor G, Mekahel K, Atias N, Gilad S, Sharan R, Levy C, Kadener S, et al. 2013. Alternative splicing regulates biogenesis of miRNAs located across exon-intron junctions. *Mol Cell* **50:** 869–881. doi:10.1016/j.molcel.2013.05.007

Meredith EK, Balas MM, Sindy K, Haislop K, Johnson AM. 2016. An RNA matchmaker protein regulates the activity of the long noncoding RNA HOTAIR. *RNA* **22:** 995–1010. doi:10.1261/rna.055830.115

Mitra R, Chen X, Greenawalt EJ, Maulik U, Jiang W, Zhao Z, Eischen CM. 2017. Decoding critical long non-coding RNA in ovarian cancer epithelial-to-mesenchymal transition. *Nat Commun* **8:** 1604. doi:10.1038/s41467-017-01781-0

Molinari C, Salvi S, Foca F, Teodorani N, Saragoni L, Puccetti M, Passardi A, Tamberi S, Avanzolini A, Lucci E, et al. 2016. miR-17-92a-1 cluster host gene (*MIR17HG*) evaluation and response to neoadjuvant chemoradiotherapy in rectal cancer. *Onco Targets Ther* **9:** 2735–2742.

Montes M, Nielsen MM, Maglieri G, Jacobsen A, Hojfeldt J, Agrawal-Singh S, Hansen K, Helin K, van de Werken HJG, Pedersen JS, et al. 2015. The lncRNA *MIR31HG* regulates $p16^{INK4A}$ expression to modulate senescence. *Nat Commun* **6:** 6967. doi:10.1038/ncomms7967

Monteys AM, Spengler RM, Wan J, Tecedor L, Lennox KA, Xing Y, Davidson BL. 2010. Structure and activity of putative intronic miRNA promoters. *RNA* **16:** 495–505. doi:10.1261/rna.1731910

Morenos L, Chatterton Z, Ng JL, Halemba MS, Parkinson-Bates M, Mechinaud F, Elwood N, Saffery R, Wong NC. 2014. Hypermethylation and down-regulation of *DLEU2* in paediatric acute myeloid leukaemia independent of embedded tumour suppressor *miR-15a/16-1*. *Mol Cancer* **13:** 123. doi:10.1186/1476-4598-13-123

Nakadai T, Fukuda A, Shimada M, Nishimura K, Hisatake K. 2015. The RNA binding complexes NF45-NF90 and NF45-NF110 associate dynamically with the c-*fos* gene and function as transcriptional coactivators. *J Biol Chem* **290:** 26832–26845. doi:10.1074/jbc.M115.688317

Ng SY, Bogu GK, Soh BS, Stanton LW. 2013. The long noncoding RNA *RMST* interacts with SOX2 to regulate neurogenesis. *Mol Cell* **51:** 349–359. doi:10.1016/j.molcel.2013.07.017

Nguyen ED, Balas MM, Griffin AM, Roberts JT, Johnson AM. 2018. Global profiling of hnRNP A2/B1-RNA binding on chromatin highlights lncRNA interactions. *RNA Biol* **15:** 901–913. doi:10.1080/15476286.2018.1474072

Noh JH, Kim KM, McClusky WG, Abdelmohsen K, Gorospe M. 2018. Cytoplasmic functions of long noncoding RNAs. *Wiley Interdiscip Rev RNA* **9:** e1471. doi:10.1002/wrna.1471

Paz I, Kosti I, Ares M Jr, Cline M, Mandel-Gutfreund Y. 2014. RBPmap: a web server for mapping binding sites of RNA-binding proteins. *Nucleic Acids Res* **42:** W361–W367. doi:10.1093/nar/gku406

Pertea M, Pertea GM, Antonescu CM, Chang TC, Mendell JT, Salzberg SL. 2015. StringTie enables improved reconstruction of a transcriptome from RNA-seq reads. *Nat Biotechnol* **33:** 290–295. doi:10.1038/nbt.3122

Pianigiani G, Licastro D, Fortugno P, Castiglia D, Petrovic I, Pagani F. 2018. Microprocessor-dependent processing of splice site overlapping microRNA exons does not result in changes in alternative splicing. *RNA* **24:** 1158–1171. doi:10.1261/rna.063438.117

Polioudakis D, Bhinge AA, Killion PJ, Lee BK, Abell NS, Iyer VR. 2013. A Myc-microRNA network promotes exit from quiescence by suppressing the interferon response and cell-cycle arrest genes. *Nucleic Acids Res* **41:** 2239–2254. doi:10.1093/nar/gks1452

Profumo V, Forte B, Percio S, Rotundo F, Doldi V, Ferrari E, Fenderico N, Dugo M, Romagnoli D, Benelli M, et al. 2019. *LEADeR* role of *miR-205* host gene as long noncoding RNA in prostate basal cell differentiation. *Nat Commun* **10:** 307. doi:10.1038/s41467-018-08153-2

Ramirez F, Ryan DP, Gruning B, Bhardwaj V, Kilpert F, Richter AS, Heyne S, Dundar F, Manke T. 2016. deepTools2: a next generation web server for deep-sequencing data analysis. *Nucleic Acids Res* **44:** W160–W165. doi:10.1093/nar/gkw257

Raveh E, Matouk IJ, Gilon M, Hochberg A. 2015. The H19 long noncoding RNA in cancer initiation, progression and metastasis—a proposed unifying theory. *Mol Cancer* **14:** 184. doi:10.1186/s12943-015-0458-2

Ritchie ME, Phipson B, Wu D, Hu Y, Law CW, Shi W, Smyth GK. 2015. limma powers differential expression analyses for RNA-sequencing and microarray studies. *Nucleic Acids Res* **43:** e47. doi:10.1093/nar/gkv007

Robinson MD, McCarthy DJ, Smyth GK. 2010. edgeR: a Bioconductor package for differential expression analysis of digital gene expression data. *Bioinformatics* **26:** 139–140. doi:10.1093/bioinformatics/btp616

Schmitt AM, Chang HY. 2016. Long noncoding RNAs in cancer pathways. *Cancer Cell* **29:** 452–463. doi:10.1016/j.ccell.2016.03.010

Shih JW, Chiang WF, Wu ATH, Wu MH, Wang LY, Yu YL, Hung YW, Wang WC, Chu CY, Hung CL, et al. 2017. Long noncoding RNA *LncHIFCAR/MIR31HG* is a HIF-1α co-activator driving oral cancer progression. *Nat Commun* **8:** 15874. doi:10.1038/ncomms15874

So WK, Cheung TH. 2018. Molecular regulation of cellular quiescence: a perspective from adult stem cells and its niches. *Methods Mol Biol* **1686:** 1–25. doi:10.1007/978-1-4939-7371-2_1

Steiman-Shimony A, Shtrikman O, Margalit H. 2018. Assessing the functional association of intronic miRNAs with their host genes. *RNA* **24:** 991–1004. doi:10.1261/rna.064386.117

Su W, Feng S, Chen X, Yang X, Mao R, Guo C, Wang Z, Thomas DG, Lin J, Reddy RM, et al. 2018. Silencing of long noncoding RNA *MIR22HG* triggers cell survival/death signaling via oncogenes YBX1, MET, and p21 in lung cancer. *Cancer Res* **78:** 3207–3219.

Suh EJ, Remillard MY, Legesse-Miller A, Johnson EL, Lemons JM, Chapman TR, Forman JJ, Kojima M, Silberman ES, Coller HA. 2012. A microRNA network regulates proliferative timing and extracellular matrix synthesis during cellular quiescence in fibroblasts. *Genome Biol* **13:** R121. doi:10.1186/gb-2012-13-12-r121

Sun Q, Hao Q, Prasanth KV. 2018a. Nuclear long noncoding RNAs: key regulators of gene expression. *Trends Genet* **34:** 142–157. doi:10.1016/j.tig.2017.11.005

Sun Q, Tripathi V, Yoon JH, Singh DK, Hao Q, Min KW, Davila S, Zealy RW, Li XL, Polycarpou-Schwarz M, et al. 2018b. MIR100 host gene-encoded lncRNAs regulate cell cycle by modulating the interaction between HuR and its target mRNAs. *Nucleic Acids Res* **46:** 10405–10416. doi:10.1093/nar/gky696

Sun T, Du SY, Armenia J, Qu F, Fan J, Wang X, Fei T, Komura K, Liu SX, Lee GM, et al. 2018c. Expression of lncRNA *MIR222HG* co-transcribed from the *miR-221/222* gene promoter facilitates the development of castration-resistant prostate cancer. *Oncogenesis* **7:** 30. doi:10.1038/s41389-018-0039-5

Tseng YY, Moriarity BS, Gong W, Akiyama R, Tiwari A, Kawakami H, Ronning P, Reuland B, Guenther K, Beadnell TC, et al. 2014. PVT1 dependence in cancer with MYC copy-number increase. *Nature* **512:** 82–86. doi:10.1038/nature13311

Valcourt JR, Lemons JM, Haley EM, Kojima M, Demuren OO, Coller HA. 2012. Staying alive: metabolic adaptations to quiescence. *Cell Cycle* **11:** 1680–1696. doi:10.4161/cc.19879

Venkatraman A, He XC, Thorvaldsen JL, Sugimura R, Perry JM, Tao F, Zhao M, Christenson MK, Sanchez R, Yu JY, et al. 2013. Maternal imprinting at the *H19-Igf2* locus maintains adult haematopoietic stem cell quiescence. *Nature* **500:** 345–349. doi:10.1038/nature12303

Wang KC, Chang HY. 2011. Molecular mechanisms of long noncoding RNAs. *Mol Cell* **43:** 904–914. doi:10.1016/j.molcel.2011.08.018

Watanabe T, Sato T, Amano T, Kawamura Y, Kawamura N, Kawaguchi H, Yamashita N, Kurihara H, Nakaoka T. 2008. *Dnm3os*, a non-coding RNA, is required for normal growth and skeletal development in mice. *Dev Dyn* **237:** 3738–3748. doi:10.1002/dvdy.21787

Westholm JO, Lai EC. 2011. Mirtrons: microRNA biogenesis via splicing. *Biochimie* **93:** 1897–1904. doi:10.1016/j.biochi.2011.06.017

Wu H, Sun S, Tu K, Gao Y, Xie B, Krainer AR, Zhu J. 2010. A splicing-independent function of SF2/ASF in microRNA processing. *Mol Cell* **38:** 67–77. doi:10.1016/j.molcel.2010.02.021

Wu CL, Wang Y, Jin B, Chen H, Xie BS, Mao ZB. 2015. Senescence-associated long non-coding RNA (*SALNR*) delays oncogene-induced senescence through NF90 regulation. *J Biol Chem* **290:** 30175–30192. doi:10.1074/jbc.M115.661785

Wu TH, Shi L, Adrian J, Shi M, Nair RV, Snyder MP, Kao PN. 2018. NF90/ILF3 is a transcription factor that promotes proliferation over differentiation by hierarchical regulation in K562 erythroleukemia cells. *PLoS ONE* **13:** e0193126. doi:10.1371/journal.pone.0193126

Wu TH, Shi L, Lowe AW, Nicolls MR, Kao PN. 2019. Inducible expression of immediate early genes is regulated through dynamic chromatin association by NF45/*ILF2* and NF90/NF110/*ILF3*. *PLoS ONE* **14:** e0216042. doi:10.1371/journal.pone.0216042

Xu J, Meng Q, Li X, Yang H, Xu J, Gao N, Sun H, Wu S, Familiari G, Relucenti M, et al. 2019. Long noncoding RNA MIR17HG promotes colorectal cancer progression via miR-17-5p. *Cancer Res* **79:** 4882–4895. doi:10.1158/0008-5472.CAN-18-3880

Yao G. 2014. Modelling mammalian cellular quiescence. *Interface Focus* **4:** 20130074. doi:10.1098/rsfs.2013.0074

Yu G, Wang LG, Han Y, He QY. 2012. clusterProfiler: an R package for comparing biological themes among gene clusters. *OMICS* **16:** 284–287. doi:10.1089/omi.2011.0118

Yuan J, Tan L, Yin Z, Zhu W, Tao K, Wang G, Shi W, Gao J. 2019. MIR17HG-miR-18a/19a axis, regulated by interferon regulatory factor-1, promotes gastric cancer metastasis via Wnt/β-catenin signalling. *Cell Death Dis* **10:** 454. doi:10.1038/s41419-019-1685-z

Yusuf I, Fruman DA. 2003. Regulation of quiescence in lymphocytes. *Trends Immunol* **24:** 380–386. doi:10.1016/S1471-4906(03)00141-8

Ziegler C, Kretz M. 2017. The more the Merrier—complexity in long non-coding RNA loci. *Front Endocrinol (Lausanne)* **8:** 90. doi:10.3389/fendo.2017.00090